Anticancer activity of silver nanoparticles embedded in porous starch as a potential delivery system

Submitted in complete fulfilment for the Degree of Master of Applied Sciences (Food Science and Technology) in the Department of Biotechnology and Food Science, Durban University of Technology, Durban, South Africa

Naaznee Mohan

February 2024

PROMOTER/ SUPERVISOR : Prof J.J. Mellem

REFERENCE DECLARATION

I, Naaznee Mohan – 21507973 and Prof J.J. Mellem do hereby declare that in respect of the following dissertation:

Title: **Anticancer activity of silver nanoparticles embedded in porous starch as a potential delivery system**

1. As far as we ascertain:

a) no other similar dissertation exists;

b) the only similar dissertation(s) that exist(s) is/are referenced in my dissertation as follows:

_____

_____

_____

2. All references as detailed in the dissertation are complete in terms of all personal communication engaged in and published works consulted.

16 February 2024

Signature of student **Date**

16 February 2024

Signature of promoter/ supervisor **Date**

AUTHORS DECLARATION

This study presents original work by the author. It has not been submitted in any form to another academic institution. Where use was made of the work of others, it has been duly acknowledged in the text. The research described in this dissertation was carried out in the Department of Biotechnology and Food Science, Faculty of Applied Sciences, Durban University of Technology, South Africa, under the supervision of **Prof J.J. Mellem**.

Student's signature

ACKNOWLEDGEMENTS

A heart-filled thanks for all the help and support from:

1. The science *Gods*.
2. Family: My parents, sister, brother-in-law and my Yasvir Brahama Deva.
3. Durban University of Technology (Department of Biotechnology and Food Science): Professor John Mellem, Dr Depika Dwarka, Dr Shivon Sipahli, Viruska Jaichand and Sonaal Ramsookmohan.
4. NRF

RESEARCH OUTPUTS

- **Mohan, N.** and Mellem, J. **2022**. Structural and physicochemical characterization of porous starch prepared by enzymatic hydrolysis, solvent-exchange, and freeze-thaw cross-linking treatments. *International Journal of Food science and Technology*. *57* (4), 2356-2364. [IF: 3.713]

PREFACE

The following dissertation is organized into five chapters and is presented as follows:

Chapter 1:

Introduction (describes problem statement, aims and contribution to knowledge relating to research).

Chapter 2:

Literature review (review of previous related studies and potential knowledge gaps).

Chapter 3: (Research objective 1):

Structural and physicochemical characterization of porous starch prepared by enzymatic hydrolysis, solvent-exchange, and freeze-thaw cross-linking treatments

Chapter 4 (Research objective 2):

Anti-cancer potential of silver nanoparticles embedded in porous starch

Chapter 5:

Summary and conclusions (general discussion of key research findings, limitations, recommendations and future work).

TABLE OF CONTENTS

ABSTRACT

Silver nanoparticles have been proven to have anticancer abilities but they have been known to agglomerate and become toxic. Therefore, various studies have been conducted to explore ways of preventing aggregation using biopolymers such as starch. This study makes use of *Lablab purpureus* (hyacinth bean) porous starch to biosynthesize and encapsulate silver nanoparticles and then test its anticancer potential. Porous starches were produced from hyacinth bean using three different techniques. These were compared against the native starch with silver nanoparticles, then synthesized and encapsulated using the porous starch. In comparison to the native starch, the porous starches made through solvent exchange and enzyme hydrolysis had similar outcomes with granules exhibiting pores, as shown by the structural and chemical characteristics. The lack of pasting properties and extremely distinct chemical and structural graphs of the porous starch, produced by freeze-thaw procedures, may be related to the presence of mercaptosuccinic acid. It was decided to employ porous starch made by solvent-exchange (SE) for the manufacture of silver nanoparticles as it contained resistant starch. Nanoparticles were produced using the porous starch from solvent-exchange, characterised and tested for their anticancer potential. Silver nanoparticles were indicative of a colour change from clear to brown, as well as, the characteristic peak at 425 nm for silver nanoparticle formation. Silver nanoparticles were implanted into porous starch at a size of around 50 nm, as further evidenced by the particle size distribution and TEM images of spherical granules with dark spots within. The zeta potential for the silver nanoparticles was -34 mV, thereby indicating that aggregation was minimized and particles were stable. The nanoparticles demonstrated less cytotoxicity in the human colon (CACO) and cervical (HELA) cancer cell lines, but more inhibition in the human breast (MCF-7) cancer cell line than the positive control camptothecin. The human muscle (C2C12), normal cell line's capacity to sustain cell viability for silver nanoparticles demonstrated that AgNP were not toxic. However, to maximize the potential of the silver nanoparticles implanted in porous starch, more research is necessary.

Chapter 1: Introduction

Cancer is one of the top causes of mortality in the world associated with many cancer patients finding their treatment to be difficult and stressful. According to WHO data from 2015 (Bray *et al.*, 2018), cancer is within the top two leading causes of death before the age of 70 in 91 of 172 countries. In another 22 nations, it ranks third or fourth in terms of the primary causes of death before the age of 70. In a study by Buttacavoli *et al.* (2018) it was found that many anticancer drugs do not reach their target sites in sufficient quantities to have a positive pharmacological effect without irreparably harming healthy tissues and cells with new and efficient therapies still being researched. Porous starch has demonstrated qualities that make it suitable for use in medication delivery systems capable of being used to improve a substance's stability and water solubility or dissolve difficult-to-dissolve drugs as well as having a large specific surface area, which contributes to its strong adsorption ability (Sujka *et al.* 2018).

Studies have shown that there are anti-cancerous characteristics in silver nanoparticles. However, numerous studies have also demonstrated that elevated reactive oxygen species (ROS) levels result in AgNP toxicity, with *in vivo* investigations potentially able to demonstrate that elevated ROS levels promote cell death-regulating pathways, such as p53, protein kinase B (AKT), and mitogen-activated protein kinase (MAPK) signalling apoptotic pathways (Li *et al.*, 2016). In a separate study, AgNPs were found to have strong *in vitro* cytotoxicity and an anticancer impact against colorectal cancer cells when they were conjugated to several colorectal medicines (Barabadi *et al.*, 2019). It was successfully used to bio-synthesise silver nanoparticles using *Piper nigrum*, which raises the possibility of therapeutic applications for these nanoparticles in cancer studies. The antitumor effect of biosynthesised AgNPs was dose-dependent and strongly inhibited both MCF-7 and Hep-2 cells. Studying the potential of porous starch and silver nanoparticles in a delivery system, as a therapeutic agent against cancer, may provide substantial information for future treatment methods.

The bioavailability and solubility of the anticancer drug, paclitaxel, loaded into porous starch as nanoparticles were compared to paclitaxel loaded into porous starch and raw paclitaxel in a study by Wang *et al.* (2019).

The paclitaxel's improved bioavailability and solubility, due to the nanoparticles placed into the porous starch, suggest a more potent mechanism of action for the anticancer drug. Zhang *et al*. (2013) studied a unique delivery strategy that combined the benefits of porous starch with a self-assembled nano-carrier in order to increase the oral absorption of lipophilic medicines. This effective delivery approach shows the potential for increasing oral bioavailability of lipophilic medications more than 10 times over the standard free drug solution.

Chapter 2: Literature review

2.1. Cancer development and causes

Cancer occurs when there is an abnormal division and uncontrolled growth of cells, altering their genes with numerous variables, including a mix of internal, genetic, environmental, and external influences, contributing to the development of cancer cells (Figure 2.1).

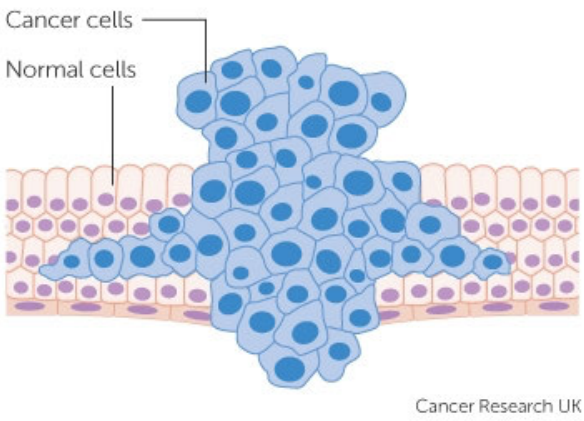

Figure 2.1: Cancer development (Cancer-Research-UK, 2023).

Cancer develops when an altered cell becomes malignant and forms a mass of neoplastic cells (Figure 2.2). There are three stages in the development of cancer which need to be considered when administering pharmacologically active agents: initiation, promotion and progression (Rather and Bhagat, 2018).

Figure 2.2: Stages in cancer development and how chemo-preventative agents can interfere (Rather and Bhagat, 2018).

In the past, cancer was linked to the professions that people have, however over the last several years' advancement within the field of science have shown that viruses are also capable of causing cancer in people. Human T-cell lymphotropic virus, hepatitis B, HIV, hepatitis C virus, Human Papillomavirus (HPV), Epstein-Barr virus, and human herpesvirus 8 are all known to cause cancer in people, according to the International Agency for Research on Cancer (IARC) (Blackadar, 2016). Sunlight, medication, nicotine, alcohol, hormones, fungi, parasites, plants, salted wood dust, fish, and bacteria are a few more carcinogens that have been listed by the IARC. The World Cancer Research Fund and the American Institute for Cancer Research have found more factors that contribute to cancer, such as beta-carotene, processed foods, red meat, obesity, low-fibre diets, higher adult height, and sedentary lifestyles (Blackadar, 2016).

2.1.1. Consequences of cancer

Over 19 million people received a cancer diagnosis in 2020, and it is predicted that there will be over 10 million cancer-related deaths globally (Sung *et al.*, 2021). Statistics show that by 2040, there would likely be close to 28 million additional cases and 16 million fatalities, respectively (Ferlay *et al.*, 2021). In 2019, the cost of cancer treatment alone in the globe was estimated to be US$1.2 trillion, or roughly 2% of the world's Gross National Product (GNP). The low to middle income countries (LMICs) are responsible for 80% of the world's cancer cases, but since they get just 5% of global funding to fight the illness, they will always lag behind in efforts to provide their population access to high-quality cancer care (Mao *et al.*, 2022).

Additionally, these nations will not continue to work together to meet the 2030 WHO Sustainable Development Goal Target, which seeks to reduce by one-third the premature death rate from non-communicable illnesses, including cancer, in comparison to rates from 2015. Owing to delayed diagnosis, restricted access to therapeutic treatments, and a lack of access to high-quality care, nations with poor human development indices (a summary assessment of major aspects impacted by sustainability and fairness) have much higher rates of premature death (Mao *et al.*, 2022).

2.1.2. Cytotoxicity

A cytotoxic agent may be described as a substance that destroys cells, including cancer cells. Cancer cells shrink and/ or stop growing when exposed to cytotoxic materials. The extent to which a chemical component or substance may destroy a cell is known as cytotoxicity (Lui and Pope, 2020). Cytotoxic drugs administered in chemotherapy is often used to treat cancer but there are various undesirable side effects due to the drugs targeting both healthy and cancerous cells (Nussbaumer *et al.*, 2011). Cells in culture are usually used in cytotoxicity assays. These tests involve the administration of test chemicals to the cells, followed by an incubation period during which a marker is evaluated to determine the number of viable cells present in relation to both positive (toxin) and negative (vehicle) treatment controls. These stages can all be very revealing, in addition to counting the number of live cells, distinguishing both cytotoxicity and cytostasis or growth arrest, as well as counting the number of dead cells that have gathered over the duration of the experiment. In some cases, estimating the total quantity of dead cells that have accumulated is more accurate than detecting a reduction in a marker used to evaluate the viable cell population (Riss *et al.*, 2019).

Carbohydrates have recently gained popularity in their use for drug delivery systems due to their beneficial properties. Starch especially have been used due to their biocompatibility, affordability, environmentally friendly and readily available nature (Sivamaruthi *et al.*, 2022). Wang *et al.* (2019) studied the cytotoxicity of paclitaxel loaded into porous starch and found that the IC_{50} values of raw paclitaxel, the system of paclitaxel directly loaded into porous starch and porous starch nanoparticles in Lewis Lung Carcinoma (LLC) cells were 17 703.41±15.76, 95.10±5.32 and 85.68±7.38 μM, respectively. This indicated that the nanoparticles had higher inhibitory abilities than the paclitaxel loaded into porous starch. Biosynthesis which includes the use of carbohydrates and silver nanoparticles have been more favoured over chemical synthesis methods recently, due to simplicity and environmental conscious factors (Algotiml *et al.*, 2022). In a study where silver biogenic nanoparticles were encapsulated by starch, it was found that the biogenic nanoparticles were more cytotoxic to HEK293 cells than the starch encapsulated silver biogenic nanoparticles (Saravanakumar *et al.*, 2021). These findings were also supported by other studies which found that a starch-silver-nanocomposite had cytotoxic behaviour on MCF-7 cancer cells whilst having little to no damage to normal cells (Valera-Zaragoza *et al.*, 2020).

2.2. Prevalence of cancer

Lung cancer accounts for 11.6% of all cancer diagnoses, followed by female breast cancer (11.6%), colorectal cancer (10.2%), and other cancers. It has been found that 18.4% of all cancer-related deaths are attributable to lung cancer, followed by colorectal cancer (9.5%) and stomach cancer (8.2%)(WHO, 2020). Cancer occurrence and outcomes are influenced by factors of health, which include biological characteristics, physical and social settings, and financial status. For instance, in nations of greater Human Development Indexes, tobacco smoking is more common among lower socioeconomic categories, leading to 60-90% higher incidence of tobacco-related malignancies. Variations in alcohol and tobacco use, poor diet, obesity, and inactivity can all contribute to the unequal distribution of cancer incidences by socioeconomic position. Figure 2.3 shows how environmental variables play a role in cancer socioeconomic inequality (WHO, 2020).

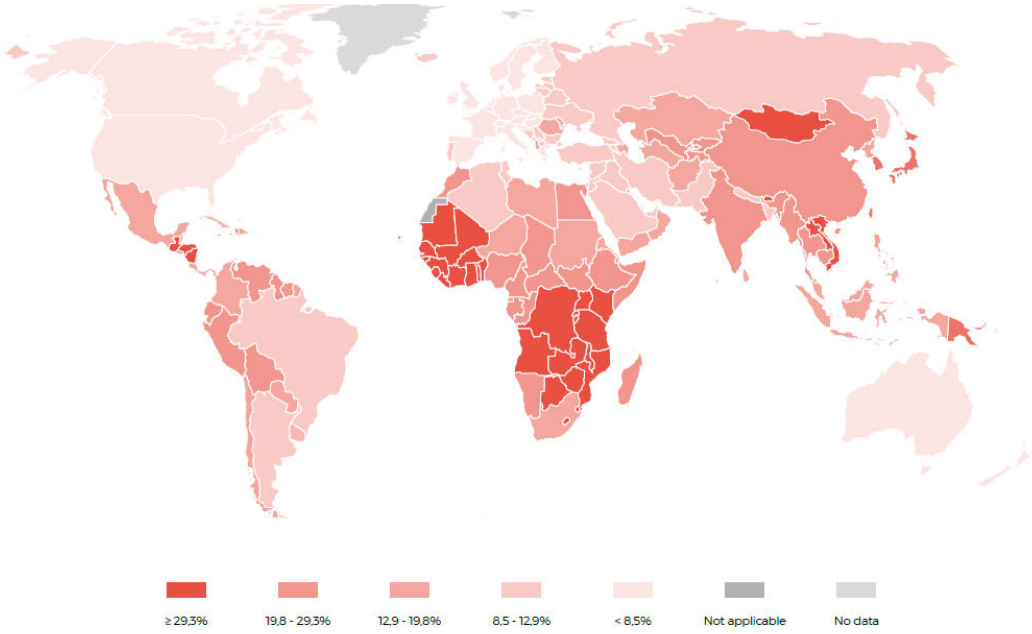

Figure 2.3: Prevalence of cancer in different areas globally, 2018 (WHO 2020).

The provinces of Gauteng and KwaZulu-Natal had the largest number of cancer fatalities in 2014, but not the highest age-standardized mortality rates, according to a study by Made *et al.* (2017) which reported rates of cancer in South Africa from 2014. Oesophageal cancer was the most prevalent type of cancer in the Eastern Cape, whereas lung and breast cancer were the most common types in the Western and Northern Capes.

The second-largest continent in terms of population is the African continent with 54 nations spread across five areas (Western, Northern, Middle, Southern, and Eastern Africa), together with a diverse population in terms of both geography and culture. African populations show significant variation in breast cancer (MCF-7) rates which is currently a major global health concern. According to the Global Cancer Observatory, there were 2.1 million instances of breast cancer in women worldwide in 2018 and it was the second-leading factor in women's cancer-related deaths. Despite being relatively low, the prevalence of breast cancer in Africa is quickly increasing, particularly in sub-Saharan Africa (SSA). It is anticipated that breast cancer in SSA in 2030 will double that of results from 2012. Sub-Saharan Africa includes a number of LMICs, many of which are in West Africa and have low gross domestic products (GDPs) per capita and human development indices (Nwagu *et al.*, 2021).

The fourth most common cancer in women diagnosed globally is cervical cancer (HELA), which is particularly widespread in LMIC countries such as South Africa (SA), India, China, and Brazil. In 2018, there were approximately 311,000 cervical cancer-related fatalities and 569,000 new instances of the disease globally (Hull *et al.*, 2020b). Overall, between 87 and 90% of fatalities and 84% of new cases are reported in LMICs. However, areas with a high socioeconomic level also frequently experience HPV infections and the related cancers. In the USA, it was projected that 80 million people had HPV infection in 2008. Despite this, early death from cervical cancer affects more LMIC women than women from affluent nations. The world's highest age-standardized incidence of cervical cancer is found in SA, where there are 32 cases per 100 000 women, while Paraguay, a middle-income country, has the highest prevalence (34.2 cases per 100 000 women) and the greatest death rate (15.7 cases per 100 000 women) (Hull *et al.*, 2020b).

Each year, colorectal cancers (CACO) cause injury to approximately 25% of the population worldwide. The likelihood of acquiring an adenoma, a benign colon tumour, is roughly 20% higher than the likelihood of having colorectal cancer, which is about 5% in developed nations (Hull *et al.*, 2020a). Effective treatments have a success rate of 70-90% when the illness is contained or circumscribed; nonetheless, advanced colorectal cancer has a high mortality rate and routinely ranks among the three leading cancer-associated causes of mortality worldwide. Currently, colorectal cancer ranks third among male cancers and second among female cancers.

Mortality rates from colorectal cancer have increased in developing countries as a result of an increase in occurrence. Globally, it was anticipated that there were over 1.9 million new instances of colorectal cancer and over 930,000 deaths from the disease in 2020 (World-Health-Organization, 2023). The strongest markers of effective cancer therapy are fatality and the rate of survival, which are directly impacted by rates of prevalence, screening, and diagnosis (Hull *et al.*, 2020a).

2.3. Current treatments and side effects

Cancer therapies have a variety of side effects that can damage multiple body systems both during and after treatment (Maltser *et al.*, 2017). Pain, exhaustion, and shifts in bowel consistency are also potential side effects of surgery. Chemotherapy can also cause fatigue, neuropathy, hair loss, and digestive issues. Radiation therapy may also induce rectal pain, nausea, diarrhoea, and sexual difficulties (Barabadi *et al.*, 2019). Not only can these procedures cause side effects, but they often come at a high cost to the patients with chemotherapy effecting organs which have normal cells that proliferate quickly (Barabadi *et al.*, 2019). Since chemotherapeutic drugs act on the ability of cells to multiply themselves, some healthy cells that reproduce quickly can also be destroyed such as blood cells, hair follicle cells, cells that line the mouth, stomach, and intestine, and reproductive organ cells. These drugs attack both dividing cancer cells and healthy cells, causing DNA damage or preventing cells from entering mitosis resulting in toxic side effects (Helleday, 2017).

2.3.1. Importance of Apoptosis in cancer treatments

Apoptosis can be referred to as "programmed cell death" which is used to explain the genetic intentional elimination of cells. It is a homeostatic mechanism that keeps cell populations in tissues stable during growth and maturation. Apoptosis can be considered as a defensive mechanism to immunological responses or cell damage brought on by illness or toxic substances (Elmore, 2007). Both regular physiological processes and the maintenance of a healthy balance between cell growth and death depend on apoptosis. It is a natural, active mechanism that eliminates individual cells without harming neighbouring cells or causing inflammation. Cell shrinkage, blabbing of the plasma membrane, preservation of organelle integrity, condensation, and fragmentation of DNA are all symptoms of apoptosis, which is accompanied by phagocytosis, which destroys the apoptotic cell (Agrawal, 2019).

Apoptosis causes the cell to shrink and undergo pyknosis, which is characterised by DNA breakage, chromatin condensation, and cytoplasmic compacting. These circumstances are followed by the plasma membrane blebbing, which results in the nucleus breaking (karyorrhexis). As a result, the cells continue to divide into fragments with the cytoplasm packed tightly with organelles as they separate from the tissue around them. These little, apoptotic bodies-like things then begin to bloom. The release of cell surface indicators (phosphatidylserine) from the cellular membrane makes it easier for macrophages and parenchyma to phagocytose these substances, thus allowing for further destruction and prevents necrosis (Carneiro and El-Deiry 2020; Denecker *et al.* 2008; Obeng 2021).

Protein cleavage, DNA cleavage, and phagocytic degradation may all be thought of as biochemical processes that result from the aforementioned circumstances. The last stage of this process appears to be entirely dependent on caspase. The cysteine protease known as caspase is a cysteine dependent aspartate specific protease. When it is activated it cleaves aspartic residue. These are proenzymes that are latent and, when activated, usually cause other pro-caspase to begin a cascade of proteases and carry out various cell killing processes. Apoptotic caspase, which comprises the initiators (-2,-8,-9,-10), effectors (-3,-6, 7), also known as executioners, and inflammatory caspases (-1,-4, 5), which are crucial for cytokine processing during inflammation, total around 18 in number. There are other caspases 11, 12, 13, and 14, each of which is known to behave in a distinct way. The 11 and 12 are demonstrated to control cytokine maturation and cytotoxicity during septic shock, with both of these having a role in apoptosis. The bovine-derived gene caspase 13 can carry out apoptosis when triggered by caspase 8, but it is also known that it is crucial for deactivating a number of proteins that are essential for life. However, it is known that caspase 14 participates in epidermal differentiation (Carneiro and El-Deiry, 2020, Denecker *et al.*, 2008, Obeng, 2021).

It is believed that caspase-14 is necessary for the efficient cornification of (pro) filaggrin. Due to the formation of tissue transglutaminase, which causes inter-nucleosomal DNA cleavage and the generation of many fragments of DNA with a typical base pair length of 180-200, protein crosslinking also acts as a biological mechanism for causing apoptosis. This DNA ladder may be seen on agarose gel electrophoresis, however, the process promotes the disintegration of specific cells, including macrophages and cells from parenchyma, under the condition that the cell surface indicators (phosphatidylserine) dissolve.

One of the intrinsic or extrinsic paths is responsible for carrying out these metabolic processes. The two groups into which the intrinsic pathway may be divided are the endoplasmic reticulum pathway and the mitochondrial pathway (Carneiro and El-Deiry, 2020, Denecker *et al.*, 2008, Obeng, 2021).

2.3.2. Apoptotic pathways

Apoptosis is mostly explained by two processes. The first pathway, sometimes referred to as "the intrinsic or mitochondrial pathway, results in the release of cytochrome c from the mitochondria and the activation of death signals when it is active". The second pathway, often known as the extrinsic or cytoplasmic pathway, is activated by the FAS death receptors, a subfamily of the tumour necrosis factor (TNF) receptor super family. Both mechanisms activate the caspase protease cascade, which cleaves regulatory and structural components and eventually causes cell death. Figure 2.4 illustrates how the pathways are also interwoven. The BCL-2 family protein overexpression in the intrinsic route may suppress extrinsic mediated apoptosis, whereas TNF- may boost NF-B expression and drive anti-apoptotic BCL-2 family members (Agrawal, 2019, Carneiro and El-Deiry, 2020, D'Arcy, 2019).

Shrinkage, blebbing, and other morphological alterations are some of the characteristics of apoptosis. Morphological alterations are also indicative of necrosis, although they are brought on by distinct circumstances and mechanisms. With regard to apoptosis, their technique for detection has changed through time as a result of changes in how apoptosis is generally understood. Prior studies included morphological analysis that preceded the DNA degradation process, nuclease testing for structural and functional changes, specific biochemical modifications, and flow cytometry (Carneiro and El-Deiry, 2020, Obeng, 2021).

The intrinsic mitochondrial pathway involves a number of internal cellular processes that take place within the mitochondria. Numerous chemicals, such as toxins, hormones, viral infections, radiation, hypoxia, growth factors, and hyperthermia, which increases the permeability of the mitochondrial intermembrane, can activate this system. Pro-apoptotic proteins are also released during this process and enter the cytosol via the intermembranes. Caspase-9 and apaf-1 (apoptotic protease activating factor-1) are bound by cytochrome c in the cytoplasm to form the "apoptosome" complex (Agrawal, 2019, Carneiro and El-Deiry, 2020, Denecker *et al.*, 2008, Obeng, 2021) .

Intracellular organelles are included in the intrinsic endoplasmic reticulum (ER) pathway which play a role in protein synthesis, modification, and folding and translocation. The ER's capacity to fold proteins can be interfered with if its function is hindered. The unfolding protein response (UPR), which is generally triggered by an ER state that is stressed, restores protein homeostasis.

Apoptosis often occurs through either an intrinsic or an extrinsic mechanism when the UPR activity fails. The extrinsic path causes cells to undergo apoptosis through the mediation of a relationship between death ligands and death receptors. The family of death receptors that these accumulating findings point to is believed to be represented by the tumour necrosis factor (TNF), which also comprises the Fas ligands (Fas-l) and the TNF-related apoptosis inducing ligand (TRAIL). By interacting with the death ligands (Fas ligands, TNF ligands), the death domain/ adapter protein [Fas-associated Death Domain (FADD), TNF receptor associated death domain (TRDD)] can connect to the death receptors (Fas receptor, TNF receptors) throughout the process (Agrawal, 2019, Carneiro and El-Deiry, 2020, Denecker *et al.*, 2008, Obeng, 2021).

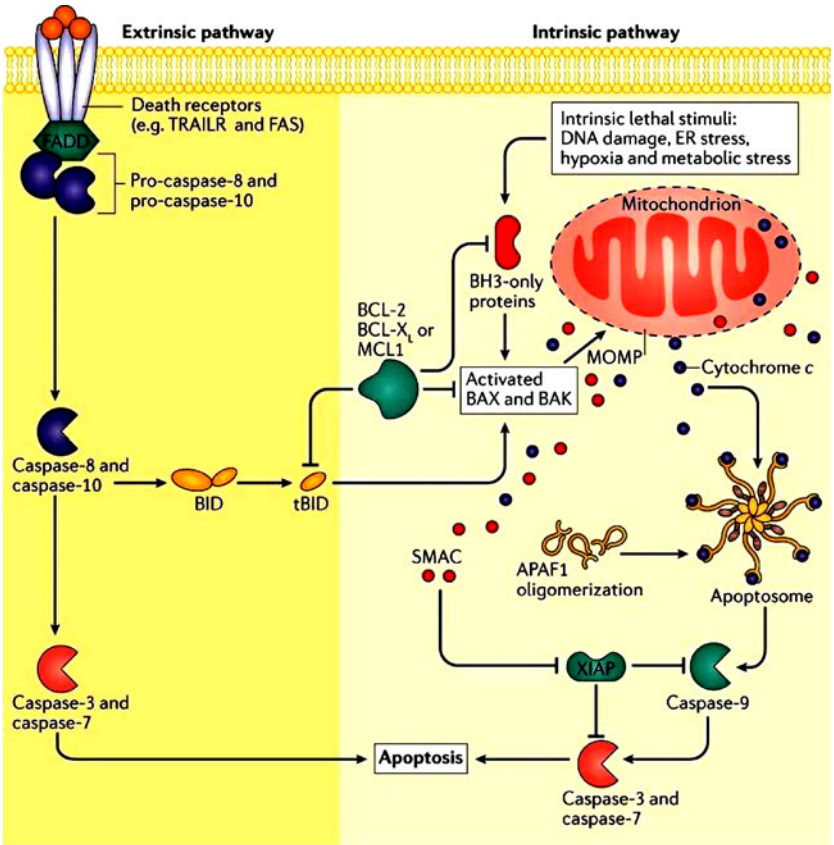

Figure 2.4: Apoptosis pathways (Agrawal 2019).

When the adapter protein/ death domain binds to the receptor ligands complex, an initiator caspase-10/ 8 can attach through its death effector domain (DED) to create the Death Inducing Signalling Complex (DISC), an active complex. Additionally, the binding and activation enable caspase-8 to transmit the death signal to an execution caspase, resulting in apoptosis. Another protein called cellular FLICE Inhibitory Protein (c-FLIP), which has the ability to bind to Death Domains, is responsible for stopping this process with an adaptor protein, stopping the activity of caspase. Therefore, it may be argued that the c-FLIP controls how the DISC operates (Agrawal, 2019, Carneiro and El-Deiry, 2020, Denecker *et al*., 2008, Obeng, 2021) .

The difficulty in recognising illnesses, particularly at an early stage when they could have been simple to treat, may be to blame for the abrupt surge. Understanding the apoptotic signals in-depth will help with the development of drugs and therapies to treat these disorders (Zhang *et al*., 2019). Additionally, it is acknowledged that the B cell/lymphoma 2 (BCL-2) family of proteins play a critical role in the control of apoptosis by functioning either independently or dependently at a site where the cell's surface and internal death signals converge, ensuring a balance (Agrawal, 2019, Carneiro and El-Deiry, 2020, Denecker *et al*., 2008, Obeng, 2021).

The term BCl-2 (b-cell lymphoma2), was originally discovered in the B-cell of human lymphomas. They are separated into pro- and anti-apoptotic groups based on their homology domain and function. These individuals have structural and functional subgroups with the BH domain. Four BH domains (BH1-4) are found in members of the anti-apoptotic protein family, whereas three or one BH domain (BH1-3) or BH3 is found in pro-apoptotic proteins, but according to current investigations, they have been found to have the BH4 domain. These proteins, which are found in the outer membrane and undergo structural modifications in response to a death signal. The anti-apoptotic members are neutralised, while the pro-apoptotic members contribute to the cell's demise. While preventing the development of the mitochondrial apoptosis induced channel (MAC), which blocks the release of cytochrome C from the mitochondrial membrane, failure of the pro-apoptotic pathway might result in cancer of the cell (Agrawal, 2019, Carneiro and El-Deiry, 2020, Denecker *et al*., 2008, Obeng, 2021).

The protein p53 is a tetramer of the tumor-suppressor protein p53, which has a protein mass of roughly 53 kDa. They participate in the development and control of the cell cycle, the induction of BCL-2 members, the permeabilization of the mitochondrial outer membrane (MOMP), receptor signalling pathways, the mediation of oxidative and endoplasmic stress, etc. However, some factors, including chemicals and viruses like the Human Papillomavirus (HPV) infection, may inactivate p53 or diminish its activity, which lessens the severity of the proliferation suppression. Apoptosis-inducing proteins like Bcl-10, Bid, Bax, Bak, Bik, Bim, Bad, and Hrk are activated upon their activation, while anti-apoptotic proteins like Bf-1, Bcl-XL, Bcl-x, B-XS, Bcl-w, and BAG are inhibited. They also allow the cell cycle to be stopped in the G-phase. Recent studies have demonstrated that flavonoids can induce apoptosis in breast cancer cells by downregulating many p53 downstream molecules, including Bcl-2 and Bcl-xl. Additionally, the fact that this process cannot happen allows for carcinogenesis (Agrawal, 2019, Carneiro and El-Deiry, 2020, Denecker *et al*., 2008, Obeng, 2021).

Eight caspase inhibitors make up the inhibitor apoptosis protein (IAP) family that include the baculoviral IAP repeat (BIR), a new domain of roughly 70-80 amino acids. They consist of the IAP-like protein 2 (ILP-2), X-linked inhibitors of apoptosis protein (XIAP), neuronal apoptosis inhibitory protein (NAIP), Survivin, BIR-containing ubiquitin-conjugating enzyme (BRUCE)/ (Apollon), livin, cellular IAP1(cIAP1), and cellular IAP 2(cIAP2). Inhibitor apoptosis proteins are able to defend cells against Fas/ caspase-8 inducing apoptosis and block the proteolysis cascade by binding their conserved domain (BIR) to the particular caspase. These IAPs are often engaged in the direct suppression of certain caspase, such caspase-3. Caspase-3,7 and -9 have been discovered to be directly inhibited by XIAP, c-IAP1, and c-IAP2. Additionally, it has been discovered that Survivin interacts with XIAP to block caspase-9, inhibiting the recruitment of Apaf1. They are also considered to be among the top five cancer-related genes, and through the overexpression of human telomerase reverse transcriptase, they have been shown to be effective in the proliferation of cancer cells. Livin has also been identified to be highly expressed in melanoma and is known to have a single BIR for the suppression of apoptosis. However, as all IAPs are known to be elevated in cancer cells, several studies have also confirmed this, demonstrating the close association between IAPS and cancer (Agrawal, 2019, Carneiro and El-Deiry, 2020, Denecker *et al*., 2008, Obeng, 2021).

2.4. Alternative cancer treatment methods

The public has long used complementary and alternative medicine (CAM) in conjunction with conventional cancer therapy to take the role of adjuvant therapies. Supplemental treatments include things such as herbs and botanicals, traditional Chinese medicine, vitamins and minerals, naturopathy, homoeopathy, and diet (Johnson *et al.*, 2018). Researchers have been creating anticancer therapeutics from diverse natural materials and their components since the middle of the 20th century. Although traditional, complementary, and integrative medicine (TCIM) is frequently utilised as a supplement to conventional medicine among populations in high-income countries (HICs), TCIM may be regarded as primary healthcare in LMICs such rural India, Brazil, and Chile.

A rising number of LMICs have started initiatives to offer conventional cancer screening, treatment, and supportive care as a result of economic development and global participation. Globally, TCIM and conventional medicine are both being used more often, but there is still friction and conflict between these two schools of thought, and systematic integration is still rare. Owing to this the expanding discipline of integrative oncology can help families, patients, and practitioners navigate between the two health care paradigms. The Society for Integrative Oncology (SIO) defines integrative oncology as a patient-centred, evidence-informed approach to cancer care that combines traditional cancer treatments with dietary changes, mind-body therapies, and herbal remedies from many traditions. Integrative oncology provides a solution and a path for providing high-quality, culturally appropriate treatment in LMICs (Mao *et al.*, 2022).

Paclitaxel and doxorubicin are some of the more popular anticancer drugs developed from plant derivatives, with anticancer drug development based on the specific target approaches of the compound. Chemotherapy is the mostly used for cancer treatment, however, cancer cell resistance to almost all forms of chemotherapy drugs and targeted medicines has become common, resulting in drug resistance responsible for approximately 80 to 90% of patient deaths, either directly or indirectly. Natural products are thus used due to their ability to increase intracellular concentrations of chemotherapeutic drugs and/or induce alternative pathways to apoptosis-induced cell death (Amaral *et al.*, 2019).

Another type of planned cell death is autophagy, which is recognised by the emergence of autophagy vacuoles in the cytoplasm and may be induced by natural compounds for cancer therapy. However there is a need for more research associated with autophagy-

inducing natural products (Lin *et al.*, 2017). Plant research has grown over the years investigating their anti-cancer and apoptotic potential. In a study by Dwarka *et al.* (2017) it was revealed that Bilirubin, an animal pigment, found in *Strelitzia nicolai,* had enhanced properties when compared to the pigment alone and that the plant exhibited potential chemo-therapeutic and preventive properties. Other research has also shown protein isolates and hydrolysates to contain anticancer and high antioxidant potential properties (Ramkisson *et al.*, 2020, Thumbrain *et al.*, 2020).

A novel treatment gaining momentum in research is nanotechnology which is the use of particles between 1 and 100 nm to develop industries. Nanomaterials created expressly for use in novel diagnostic and medication delivery technologies are used in treatment modalities in nanomedicine, which integrates nanotechnology into biomedical research (Abrahamse *et al.*, 2017). In medicine, nanoparticles are frequently utilised to increase bioavailability, as agents, or to establish novel imaging techniques, to improve therapeutic delivery, and to ensure biological system regulation for single molecules or groups of molecules (Jurj *et al.*, 2017).

2.5. Silver nanoparticles in cancer treatment

The most widely utilised nanomaterials are silver nanoparticles (AgNPs), which are also among the most significant due to their great demand as materials for consumer products. Silver nanoparticles (1-100 nm) can move the cell membrane and penetrate the nucleus, where they can interfere with genetic material resulting in genotoxicity (Arpan *et al.*, 2019). Silver nanoparticles have a greater contact-area-to-volume ratio as compared to bulk particles, which enhance their surface characteristics and improves their interaction with saliva, fluid components, mucus, and serum of the lung lining (Akter *et al.*, 2018). Silver nanoparticles can be manufactured through biological, chemical and physical means (Figure 2.5). Due to the cost of production, low yield and complicated techniques associated with physical and chemical means, biological methods which utilizes natural sources as reducing agents or stabilizers have been the most popular option (Arpan *et al.*, 2019). The genotoxicity and cytotoxicity of AgNPs is dependent on various factors such as: particle size, cell type, concentration of nanoparticle, exposure time and, the environment.

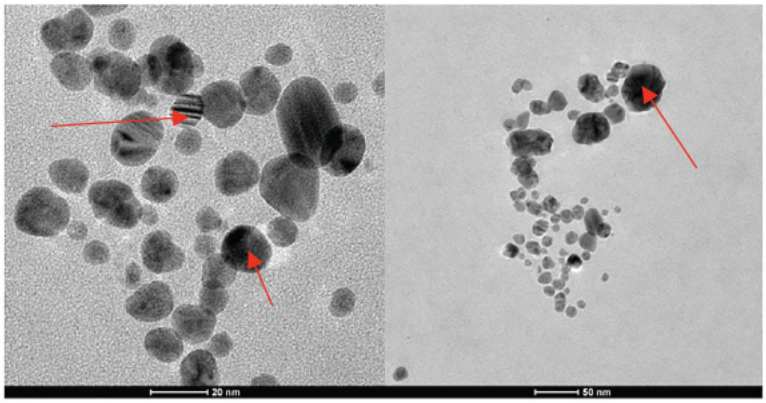

Figure 2.5: TEM images of silver nanoparticles biosynthesized (Wypij *et al.*, 2021).

Homeostasis of reactive oxygen species (ROS) is necessary for normal cell survival, therefore, signalling with ROS in low levels is capable of being used to monitor metabolic adaptation, differentiation, and cellular proliferation. Cancer cells produce more spatially localized ROS than normal cells, which hyper activates the cell signalling pathways needed for cellular transformation and tumorigenesis (Liou and Storz, 2010). Therefore, ROS generation may be a potential mechanism for AgNPs-induced toxicity via oxidative stress. Excessive ROS development by mitochondria can lead to a breakdown of the antioxidant defence mechanism, causing damage to proteins, lipids, DNA, ATP synthesis, and eventually apoptosis. Similarly, when AgNPs enter a cell, they normally contain ROS. As ROS levels rise, glutathione levels drop significantly, while lactate dehydrogenase activity (LDH) rises in the medium, resulting in apoptosis (Akter *et al.*, 2018). Standard chemotherapeutic drugs and silver nanoparticles have been used together to induce a cytotoxic effect and have shown to be successful against leukaemia, breast, lung, prostate, hepatic, cervical, skin, larynx, and colon cancer.

It has also been shown that silver nanoparticles are target specific and safe against normal cells (Vlăsceanu *et al.*, 2016). Nanoparticles may be used to develop target-specific medications for photosynthetic drug delivery that are absorbed by cancer cells and prevent any side effects associated with photosynthetic pharmaceuticals or photodynamic treatment. Research has revealed that the water solubility of photosensitizer drugs were also improved using nanomaterials. The selective accumulation of the photosensitizer pharmaceuticals in tumours was enhanced by the modification of the medications with nanoparticles that have active targeting ligands (Abrahamse *et al.*, 2017).

In a study looking at the anticancer and antioxidant properties of the black peel pomegranate extract was revealed to exhibit selective cytotoxicity against cells, meaning that they were harmful exclusively to tumour cell types. The extract also showed capacity for the biogenesis of AgNPs by converting silver ions into tiny, stable, spherical AgNPs at an extremely rapid rate without the need for heating or external accelerators (Khorrami *et al.*, 2019).

In a study that synthesised and characterised AgNPs using *Origanum onites* leaves, Caco-2 and Capan-1 cancer cell lines were significantly harmed, but mouse normal fibroblast cell lines (L929) were unaffected. The effect of the nanoparticles and extract on cell viability in Capan-1 cell lines were found to be 45.4 and 24.6%, respectively (1.0 $\mu g.mL^{-1}$) (Gecer, 2023). In a study examining the nano-toxic effects of AgNPs on normal HEK-293 cells in comparison to cancerous HeLa cell line, it was found that the cytotoxicity on the cell lines was dose-dependent. At 2.5 L/mL of the AgNPs containing hydrosol, 100% inhibition of HEK-293 cells and 75% inhibition of HeLa cells were observed (Liu *et al.*, 2021).

2.6. Production of AgNPs

Biological, chemical and physical syntheses are only a few of the processes used to create silver nanoparticles, with each technique showing advantages and downsides. During biological manufacture, the organism used works as a stabilising, reducing, or capping agent of AgNPs, reducing Ag+ to generate Ag0. Recently, there has been a growth in the utilization of biological technologies based on natural products derived from microbial and botanical sources due to their high production, affordability, and minimal toxicity in humans and the environment (Almatroudi, 2020).

Chemical procedures are advantageous because they require less complicated and handier equipment than biological alternatives. Silver ions are known to acquire electrons from the reducing agent and change into the metallic state, which then assembles to produce silver nanoparticles. Silver nitrate ($AgNO_3$) is one of the most commonly utilised silver salts due to features such as low cost when creating AgNPs chemically. Sodium borohydride is said to be an effective reducing agent for the creation of AgNPs with a size range of 5-20 nm. The most effective reducing agent, however, for the production of silver nanoparticles in the 60-100 nm size range is trisodium citrate.

Other studies have used polyvinylpyrrolidone (PVP) as a capping agent together with ethylene glycol as a reducing agent to make AgNPs which are approximately 10 nm (Dang, 2012). An aqueous solution of silver nitrate is injected in the precursor heating technique, with the reaction temperature important for reducing particle size and producing monodispersity. Comparatively, the ramping rate of the precursor injection technique, which employs a silver nitrate aqueous solution, is shown to have the biggest influence on the size of the nanoparticles (Patil *et al.*, 2012).

The physical processes of evaporation-condensation and laser ablation are used to produce AgNPs. These technologies' primary limitations are the energy used and time needed to complete the entire operation. In order to compare the size and effectiveness of colloidal particle production caused by femtosecond laser pulses versus colloidal particle creation caused by nanosecond laser pulses, Tsuji *et al.* (2002) used laser ablation to create nanosized silver particles in water. Femtosecond pulses have a considerably poorer formation efficiency than nanosecond pulses, in addition, femtosecond laser pulses produced colloids that were less scattered in size than nanosecond laser pulses did (Tsuji *et al.*, 2002).

Physical and chemical methods for producing silver nanoparticles are costly, time-consuming, and unsustainable. Since hazardous chemicals and other issues related to chemical and physical methods of manufacturing must be avoided, it is crucial to establish an ecologically and economically acceptable technique. These gaps are filled by the regulation of various biological processes, which also have numerous applications in the management of health. Fungi, bacteria, and yeast are often used in biological production techniques in addition to plant sources making this method highly well-liked for using nanoparticles in medicinal applications (Almatroudi, 2020).

2.7. Characterization of silver nanoparticles

Numerous analytical techniques, including X-ray diffractometry (XRD), scanning electron microscopy (SEM), dynamic light scattering (DLS), transmission electron microscopy (TEM), atomic force microscopy (AFM), Fourier transform infrared spectroscopy (FTIR), and others, have been used to evaluate the synthesised nanomaterials. The biological activity of AgNPs are influenced by their size, cell type, surface chemistry, dissolving rate, size distribution, efficiency of ion release, shape, particle reactivity in solution, coating or capping, and agglomeration.

Another crucial factor to be considered that is associated with cytotoxicity is the kind of reducing agents utilised to create AgNPs (Zhang *et al.*, 2016).

To determine the surface chemical properties and functional compounds in AgNPs, FTIR is utilised. This method is affordable and quick for looking at how biomolecules contribute to the conversion of silver nitrate to silver (Arpan *et al.*, 2019). One of the first stages associated with the characterisation of synthesised nanoparticles is UV-vis spectroscopy which is used to assess stability and efficacy of AgNP manufacturing. The valence and conduction bands in AgNPs are relatively close to one another, allowing electrons to effortlessly pass through them. A surface plasmon resonance (SPR) absorption band is produced as a result of the free electrons in the silver nanoparticles collectively oscillating in resonance with the light wave. The size of the particles, the dielectric medium, and the chemical environment all affect AgNPs absorption. This peak is often present in metal nanoparticles with sizes between 2 and 100 nm (Zhang *et al.*, 2016).

The popular analytical method known as X-ray diffraction (XRD) has been used for a variety of purposes, including the analysis of crystal and molecular structures, the determination of crystallinity, qualitative identification of various compounds, isomorphous substitutions, quantitative resolution of particle sizes and chemical species, etc. Any crystal will reflect X-ray radiation, causing a variety of diffraction patterns to occur which will reveal the physicochemical properties of the crystal formations. Typically, diffracted beams in a powder specimen originate from the sample and represent its structural physicochemical characteristics. As a result, XRD may be used to investigate the structural characteristics of a variety of materials.

Dynamic light scattering (DLS) can measure the zeta potential of particles and investigate the size distribution of tiny particles in solution or suspension on a scale spanning from submicron down to one nanometre. Zeta potential, a critical characteristic for characterising stability in aqueous AgNP suspensions, assesses the surface electric charge on the nanoparticle. Because of their surface charge, nanoparticles draw a layer of ions with opposing charges to their surface. The nanoparticles travel with the formed double layer of ions as they dissolve. The Zeta potential of the nanoparticles, or the net electric charge potential between the layers, typically ranges from +100 to -100 mV. The nanoparticle stability is predicted by the zeta potential (Rajeshkumar and Bharath, 2017).

Transmission electron microscopy (TEM) is a valuable, widely applied, and significant tool for accurate measurements of morphology size distribution, and particle and/or grain size for nanomaterials. According to Zhang *et al*. (2016), the distance between the lens that serves as the objective and the specimen as well as the distance between the objective lens and its image plane heavily influence the magnification of TEM.

2.8. Starch-silver Nano-delivery systems

The creation, characterisation, biocompatibility, and antibacterial activity of starch-encased silver nanoparticles (St-PF-AgNPs) were evaluated in a study by Saravanakumar *et al*. (2021). Starch-encased silver nanoparticles were created in two steps: first, biogenic silver nanoparticles were created using fungus extracts (PF-AgNPs), and then, starch was enclosed within these nanoparticles to create St-PF-AgNPs. For the PF-AgNPs, the surface plasmon resonance was discovered at 420 nm, but for the St-PF-AgNPs, it was discovered at 260 and 420 nm. The capping and encapsulating of the starch and fungal extracts in PF-AgNPs and St-PF-AgNPs were visible in the FTIR spectrum. The polydispersed, spherical, and crystalline character of PF-AgNPs and St-PF-AgNPs with significant indications of Ag were verified by the XRD and TEM-EDS. Dynamic light scattering and zeta potential measurements of the St-PFAgNPs revealed a Z-average size of 115.2 d.nm and a zeta potential of -17.8 (mV). In HEK293 cells, the cytotoxicity data showed PF-AgNPs to be more harmful than St-PF-AgNPs. Starch-encased silver nanoparticles exhibited more antibacterial efficacy against *S. aureus* than PF-AgNPs. In general, this work discovered that the PF-AgNPs' antibacterial effect was significantly enhanced by starch encapsulation. By using PF-AgNPs that are produced continuously to target damaging bacterial cells, this discovery offers a novel method for treating bacterial infections (Saravanakumar *et al*., 2021).

In a study by Wang *et al*. (2021) the impact of metal nanoparticles loaded with isoorientin (Iso), a naturally occurring flavonoid was evaluated. The structural characterisation and stability of AgNPs loaded with iso (AgNPs-Iso) were studied by UV-vis spectroscopy and zetasizer. Silver nanoparticles were synthesised using maize starch and sodium citrate using the green synthesis technique. The outcome shows that Iso (117$\pm$2.13 nm, loading efficiency: 76.60%) was effectively loaded onto AgNPs (65$\pm$0.87 nm, spheres). In a solution with a pH range of 5-9 and 0.01-0.30 M of NaCl, there are no appreciable variations in the stability of AgNPs and AgNPs-Iso.

In the *in vitro* simulation of gastrointestinal digestion, AgNPs-Iso were more stable than AgNPs. Additionally, AgNPs-Iso showed a significantly inhibitive impact on α-glucosidase and pancreatic lipase in addition to having a decreased erythrocyte hemolysis ratio and cytotoxicity. Therefore, this research might offer the fundamental justification for the further development of Type II diabetes and obesity-fighting, highly stable, and less cytotoxic AgNPs-Iso (Wang *et al.*, 2021).

In another study, cowpea starch was used to create AgNPs with the precursor silver nitrate converted to AgNPs by the free aldehyde group of the glucose residue in the amylose chain of the starch polymer. Starch served as a capping agent for AgNPs, controlling their size, shape, and dispersion characteristics. Starch's hydroxyl group, which gives it its capping capabilities, stabilises metal nanoparticles through it's inter- and intramolecular hydrogen bonds. Silver nanoparticles are more biocompatible when they are encapsulated in starch, which also increases their immunological tolerance and dispersibility and is also stated that AgNPs are not hazardous to healthy human cells. While starch alone exhibited little bactericidal action, starch stabilised AgNPs have shown strong antibacterial potential against both gram positive and negative bacterial strains, demonstrating that the antimicrobial potential may be related to the AgNPs' stabilisation with starch (Sivamaruthi *et al.*, 2022).

2.9. Porous starch

A modified starch having a lot of holes from the surface to the middle and improved characteristics is called porous starch (PS) (Benavent-Gil and Rosell, 2017a). Porosity is defined as "the ratio of pore volume to particle volume" with one- or two-sided pores as well as closed pores are possible. Meso-pores are between 2-50 nm, micro-pores are <2 nm, and macropores are >50 nm (Sujka *et al.*, 2018).

Pores are capable of enhancing the surface area that can be utilised for reactions with enzymes or chemicals. The size of the pores affects how well starch granules can absorb water and oil. Porous starch is also capable of supporting a wide range of bioactive molecules, including bacteria, enzymes, tastes, and medications (Chen *et al.*, 2020, Liu *et al.*, 2018).

2.9.1. Significance of porous starch

In the human diet, starch can be considered as one of the most important carbohydrates serving as one of the main constituents of non-animal foods. Starches serve many functions due to their technological and texturizing characteristics (Lehmann and Robin, 2007). The granules of pulse starch are frequently oval, although they can also be spherical, round, elliptical, and irregularly shaped. Amylose and amylopectin are the two main components of starch (Hoover *et al.*, 2010). The use of native starch is constrained due to its susceptibility to processing conditions such high shear rates, low pH, severe temperatures, and freeze-thaw variation, however many starch properties may be improved by isolating porous starch (Liu *et al.*, 2018).

2.9.2. Production of porous starch

Porous starch has many desirable properties such as an enhanced adsorption capacity which is highly desired in drug loading applications to increase the bioavailability of insoluble drugs (Wang *et al.*, 2019). Starch applications are restricted because of low surface area and pore volume, despite the fact that it is one of the most extensively used materials since it is an affordable, biodegradable, reusable, and ecologically benign biopolymer. Porous starch is produced by chemical, physical, or enzymatic alteration.

Chemical and enzymatic methods

Porous starch may be made chemically using several techniques such as solvent exchange, molecular insertion, and acid hydrolysis. Enzymatic hydrolysis is a reaction between raw starches and starch-hydrolysing enzymes that produce porous starch at the temperature of gelatinization of starch. After hydrolysis of the amorphous regions of starch, the result is an undestroyed starch granule with craters on the surface and/or holes that extend to the middle (Figure 2.6). α-Amylase and glucoamylase are the most commonly used enzymes to produce porous starch (Zhang *et al.*, 2012).

Starch is combined with mercaptosuccinic acid to create a combination that is first gelatinized and then freeze-dried to create a xerogel. Because mercaptosuccinic acid may break the hydrogen bonds inside starch chains, intermolecular hydrogen bonds are created between the mercaptosuccinic acid and the starch (Liu *et al.*, 2018, Bao *et al.*, 2016).

Starch xerogels have a wrinkled look as a result of the addition (during gelatinization) and evaporation (during freeze-drying) of water atoms inside the starch chains. The porous structure of starch is caused by the introduction of mercaptosuccinic acid atoms by the rupturing of hydrogen bonds inside the starch chains (Qian and McClements, 2011). The solvent- exchange method is another method to produce porous starch. Water can dehydrate from ethanol due to the hydroxyl groups on the surface of starch materials, and porous starch granules have a greater specific surface area, increasing the total number of hydroxyl groups on the surface of starch particles. The increased surface area allows for more reactive sites to be grafted with functionalized groups to enhance starch properties (Han *et al.*, 2020).

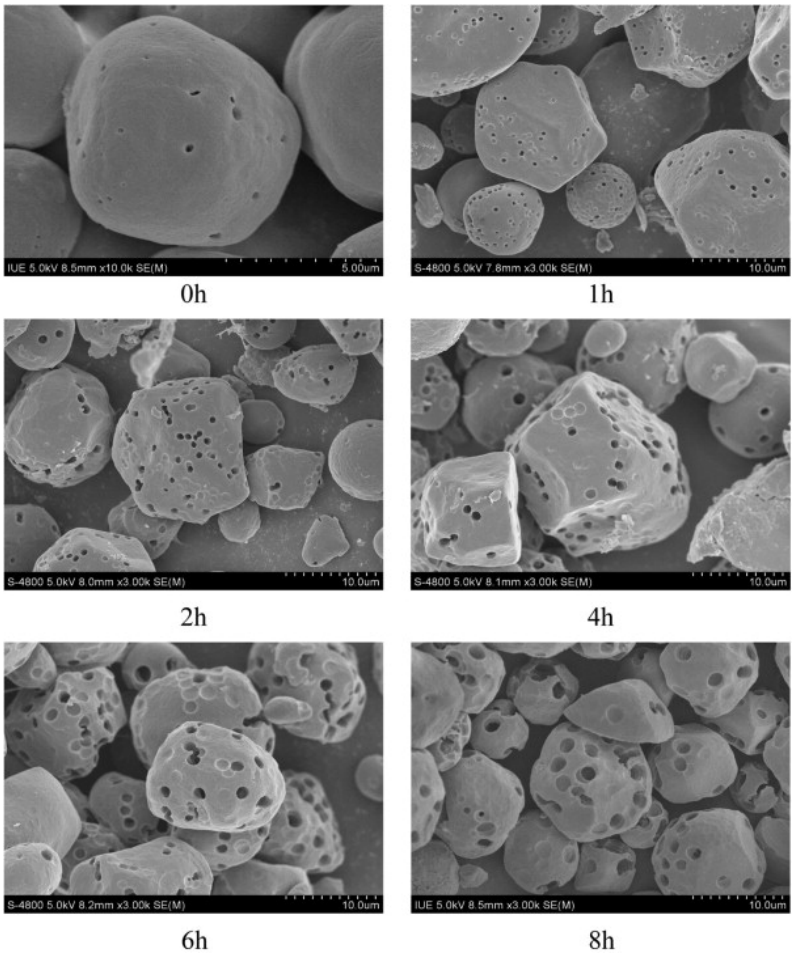

Figure 2.6: Porous starch from corn starch during 8 h treatment by glucoamylase (Chen and Zhang, 2012).

Physical methods

Through traditional physical hole-forming techniques (such as mechanical extrusion, microwave, and ultrasonic processes), porous starch may be made quickly and easily. Mechanical extrusion involves a variety of physical unit operations, such as heating, mixing, stirring, puffing, and spraying. This technique uses a significant pressure differential to spray starch paste, which quickly evaporates water and creates loose porous structures in the starch. Porous starch with enhanced porosity may be generated at temperatures of 160°C, 18% moisture content, and 200 rpm rotor speeds. Although the porosity of extracted starch is inversely linked to the water content, it has a positive correlation with temperature. Notably, mechanical extrusion-produced porous starch frequently exhibits irregular pore size. This process produces a relatively low yield of porous starch. Additionally, the high extrusion temperature (<95°C) has the potential to gelatinize starch granules and harm their structural integrity. Therefore, precooked cereal goods are typically made using the mechanical extrusion process (Chen *et al*., 2020).

The microwave approach has been employed to develop porous starch since it is both effective and ecologically safe. This technique is based on the heat effect produced by microwaves that may penetrate starch granules through "molecular friction" in an alternating electromagnetic field. Granules of swelled starch are neatly aligned in an electric field. When exposed to a microwave, starch granules can vibrate at a high frequency due to the alternating electromagnetic field's positive and negative polarities which are constantly swapped. Granules of starch convert microwave radiation into heat energy as a result. The resulting loss of heat from the starch granule surface may result in the accumulation of thermal energy. Starch granules rapidly evaporate their moisture, which results in a high pressure inside the granules (Chen *et al*., 2020).

In general, a variety of variables, including treatment time, microwave power, and starch dose, have an impact on the structure of porous starch. Despite being easy and inexpensive, the microwave approach produces porous starch with a low number of holes. Therefore, it is inefficient to produce porous starch using the microwave. Ultrasonic irradiation is a more accepted approach to prepare porous starch since it uses less energy and is easy to use. The key variables determining the pore size are the ultrasonic operating parameters, the strength, treatment time and frequency of the ultrasonic wave.

The standing wave is created when the ultrasonic wave returns to the gas-liquid interface after travelling to the starch solution. This will cause porous starch to have unequal pores, which is disadvantageous for porous starch's industrial application (Chen *et al.*, 2020).

2.9.3. Characterisation of porous starch

Differential scanning calorimetry (DSC), scanning electron microscopy (SEM), rheometry and Fourier-transform infrared (FTIR) spectroscopy are tools often used to determine the characteristics of porous starch (Liu *et al.*, 2018). The molecular structure of starch is usually determined by FTIR, through the interpretation of the absorption of characteristic peaks, the structure of starch is evaluated. It has been found that the molecular structure of porous starch obtained by an enzymatic reaction, did not change from its native state. Demonstrating that the functional groups of corn native and porous starch are comparable. However, because of the holes, which reduced the density of the starch granules, the peak intensity was less intense. According to Liu *et al.* (2018) significant peaks that describe starch include those at 1067 cm^{-1} (C-H bending), 764 cm^{-1} (C-C stretch), 3165 cm^{-1} (-CH2 deformation), and 1344 cm^{-1} (C-O-H bending and -CH2 twisting).

The morphology of the starch granules is usually determined by SEM including: the shape, number of pores and the type of surface which differ according to the sample, and method of extraction. Some studies report smooth surfaces with a round and polygonal granular shape with pores spread from the surface to the centre of the pores. The internal cavities could explain the excellent adsorption capacity characteristic in porous starch (Liu *et al.*, 2018). X-ray diffraction is used to examine the amorphous and crystalline regions of the starch. It was observed that the A-type pattern of native corn starch did not change in its porous starch but the crystallinity was increased. The sharper and higher peaks show that the majority of the enzymatic reaction's hydrolysis took place in the amorphous zone. Therefore, as a result of the enzymatic process, the amorphous area shrank and the crystalline region grew; causing maize PS to exhibit a greater crystallinity than native corn starch (Liu *et al.*, 2018).

The thermal characteristics of starch, in particular the changes in the physical states of the starch structures, are studied using DSC. Typically determined and compared during characterisation are the transition temperatures (To, Tp, and Tc), gelatinization temperature range (Tc-To), enthalpies of gelatinization (H), and peak height index (PHI).

The crystalline area may be connected to the temperature range of gelatinization due to water molecules readily flowing into the amorphous portion of starch during the endothermic reaction of gelatinization, entering the crystalline zone (Liu *et al.*, 2018).

When starch is heated up in excess water, a change in phase from order to disorder, known as gelatinization, which occurs over an ideal temperature range unique to the starch source occurs. Phase change is related to the diffusion of water into the granule, following that, water is absorbed by the amorphous background region, resulting in hydration and radial expansion of the starch granules, loss of birefringence and crystallinity, heat absorption, dissociation of double helices, and leaching of amylose. It is generally known that the gelatinization transition temperatures To (onset), Tp (peak), Tc (endset), and the enthalpy of gelatinization (ΔHgel) are all influenced by the molecular structure of the crystalline region. Instead of the quantity of crystalline area or the amylose to amylopectin ratio, it has been associated with how the short amylopectin chains are distributed within the granule.

Differential scanning calorimetry (DSC) is used to assess how well starch gelatinizes. The variable amylopectin content and distribution, degree of crystalline perfection, proportion of lipid-complexed amylose chains, and proportion of the outer "A" branches of amylopectin have all been reported as the causes of this variation in the gelatinization temperatures of legume starches (Wani *et al.*, 2016). The physicochemical properties are usually done to determine the characteristics of compounds that are suitable for: desirable coating of unappealing drugs, ingredient development; improvement and quality management of food products (Naiker *et al.*, 2019).

Starch composites consist of amylose and amylopectin, which are α-glucans and makeup 98-99% of the dry weight with the rest consisting of phosphates esterified to glucose hydroxyls, minerals, and lipids. The amount and distribution of these glucans have an effect on the physicochemical characteristics of starch. The fundamental characteristics that depend on a substance's chemical, structural, and morphological characteristics include swelling and solubility, syneresis, gelatinization, gelation, transmission, and pasting. According to Wani *et al.* (2016) the amylose concentration of legume starches range from 17.00-51.69%. The swelling and solubility index of the starch are influenced by the amorphous and crystalline areas of the starch granules.

The granules absorb water and swell when the starch dispersions are heated in water. The rise in temperature weakens the intrinsic bonds and binding forces of starch granules. The amorphous amylose component is produced as a result, increasing the surrounding medium's viscosity. A high swelling and solubility index is attributed to the low molecular weight of amylose and the shape of free starch granules. Granules of starch having complex and solid bonds inside the micellar structure and are more resistant to swelling, which lowers the solubility index. The swelling and solubility of starch granules are influenced by the ratio of amylose to amylopectin, the length, branching, and molecular weight of the chain, the micellar structure inside the granule, the presence of lipid that forms complexes with amylose, and the naturally occurring non-carbohydrate contaminants in starch molecules (Wani *et al*., 2016).

"A viscous mass consisting of a continuous phase of solubilized amylose and/ or amylopectin and a discontinuous phase of granule ghosts and fragments" (CSP) is how the term "paste" is defined (Wani *et al*., 2016). The changes in starch that take place during post-gelatinization heating are specifically related to a complex phenomenon known as "pasting." Shear force application causes further swelling and polysaccharide leaching from the starch granules, which increases viscosity. The Rapid Visco Analyzer (RVA) has been used regularly to assess the starch pasting qualities. In order to connect functionality with structural features, heating and cooling cycles are used to assess sample resistance to controlled shear. It also replicates food processing settings. A normal RVA graph for starch gelatinization follows a pattern in which viscosity first climbs to the maximum value then decreases to the lowest value as a result of the granules' disintegration when shear is applied. As a result, the breakdown and trough viscosities are used to express it. The viscosity again increases to the greatest amount known as setback as the cooling cycle progresses. Amylose content and peak viscosity have a negative association with peak viscosity and a positive correlation with the setback values. Peak time and peak viscosity are correlated with the ability of the starch granules to bind water and their ease of disintegration. These characteristics are all known to affect the product's texture and palatability (Wani *et al*., 2016).

"The amount of water held by the starch" is how the term "water absorption capacity" (WAC) is defined (Wani *et al*. 2016) and is reliant on the hydrophilic regions in the starch molecules. The WAC increases with the number of hydrophilic sites available to engage in hydrogen bonding interactions with water.

At room temperature, amylose and amylopectin chains' interactions with water are still modest, but become stronger as the temperature rises. The degree of water binding site availability among the starches, stearic factors, structural traits, the existence of hydrogen bonds, and the hydrophilic-hydrophobic balance all affect WAC. The WAC of starch suspensions may also be impacted by the physicochemical environment, which includes factors such as temperature, pH, vapour pressure, ionic strength, and the presence or absence of a surfactant. In contrast to the swelling index, WAC accounts for the fact that starch absorbs more water as the temperature rises. The amylose concentration, amylose-lipid complexes, interactions between starch chains in the amorphous and crystalline area of the granule, and the molecular makeup of amylopectin all have an impact on the swelling index of starch. As opposed to WAC, the swelling power and solubility index reveals how starch chains interact in the amorphous and crystalline areas (Wani *et al.*, 2016).

According to Wani *et al.* (2016), oil absorption capacity (OAC) is a crucial functional feature for enhancing shelf life, taste retention, and palatability. The size and form of the starch determines how physically entrapped the oil is (Verma *et al.* 2018). Due to its crucial function in preserving taste and improving the mouth feel of foods, the oil absorption capacity of flours may also be ascribed to their hydrophobicity power. This property might be leveraged to create food items with desirable ingredients (Ramsookmohan *et al.*, 2020).

Protein content and solubility are correlated with foaming and emulsifying capabilities. Because of surface-active proteins, flours can create foams. Three things are necessary for foam to form: molecular movement, penetration, and rearrangement at the air-water interface. To assess the applicability of foaming agents, foam stability is crucial to determining the capacity to sustain a foam over time (Ahmed Wani *et al.*, 2015). Emulsion stability refers to an emulsion's capacity to hold together. The maximum amount of oil that may be emulsified by protein dispersion is known as the emulsion capacity. Proteins in flours lower the interfacial energy because of the protein's adsorption at the oil-water interface and the interfacial layer's impact on the electrostatic, structural, and mechanical energy barriers that prevent the separation of the oil and water phases. Beyond the various protein compositions (soluble plus insoluble), elements other than proteins (perhaps carbohydrates) may greatly influence the ability of products like flours containing protein to emulsify (Wani *et al.*, 2016).

2.9.4. Advantages and benefits of porous starch

Starch granules may be used to encapsulate and distribute active ingredients because of their internal structure, which includes an internal channel. Porous starch has many benefits and can be used to deliver a variety of actives, including medications, vitamins, flavour compounds, and nutraceuticals, thanks to its surface pores and channels (Figure 2.7). While the starch molecules are consumed by the active components in other products or circumstances, they may be passively co-located with the active ingredients. Chemical or physical interactions take place pre to, during, and after processing depending on the starch, active components, and production circumstances (Qi and Tester, 2019). In a study to protect *L. plantarum* from various stresses without affecting its survival rate, the bacterium was enclosed in porous starch (Chen *et al*., 2020). Majzoobi *et al*. (2015) studied the enhanced functional properties of porous starch from wheat. A combined treatment of α-amylase and sonication improved the absorption properties of the wheat starch. In a study by Zhu *et al*. (2019) porous maize starch was used to deliver the anticancer drug doxorubicin using pectin/ chitosan beads. Results showed that most of the loaded drug was delivered to the colon and proved to be an effective target-specific delivery system. It also showed that oxidation-prone or low solubility drugs could be delivered using this system.

Wu *et al*. (2011) created a biodegradable porous starch foam as a carrier to improve the oral bioavailability and degradation of lovastatin, a water-insoluble medication. The porous starch foam was made using the solvent-exchange process, and lovastatin was loaded using immersion/ solvent evaporation. As compared to the crude and capsule shape, the porous starch foam successfully improved lovastatin release and oral bioavailability. Protection from the local environment (especially through the stomach), safety, dissolution enhancement, removal of the need for the liquid carrier, absorption capacity, stability, active ingredient protection (e.g. from oxidation), loading, 'metering of dose' where a small amount of is required, taste masking, and site-specificity are all advantages of using porous starches as carriers. Diffusion (a vapour or a solvent), enzymatic hydrolysis (amylases/ amyloglucosidase), and/or physical processing may all be used to release encapsulated compounds (Qi and Tester, 2019).

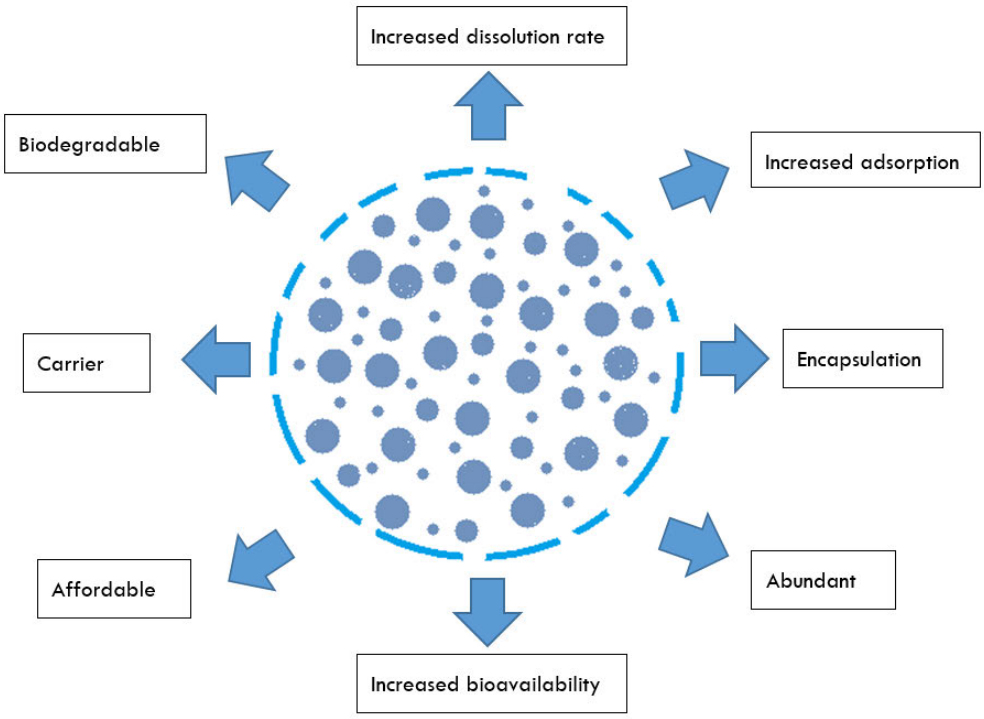

Figure 2.7: Benefits of porous starch.

Particulate carriers (mainly made of lipids and/ or polymers) and related treatments are typically included in drug delivery systems. They are made to act as drug reservoirs, change the pharmacokinetics and bio distribution of the linked medications, or both. A pleasant, inert, biocompatible, bio adhesive, and high drug-loading drug delivery device is desired. All of these requirements are met by porous starch. All significant regulatory organisations have given their formal approval for the use of starch in various oral medication delivery methods. Since starch polymer chains are hydrolysed into smaller, physiologically acceptable molecules, the drug delivery system does not need to be removed from the body after the active ingredient has been released. The capacity of a microcapsule to absorb substances and adhere to surfaces can be improved by using porous starch as a wall material (Sujka *et al.*, 2018).

2.9.5. Porous starch in the treatment of diseases

Porous starch is often studied for its use in treatments with different ways to utilise the starch such as aerogels, hydrogels, powders, etc. which are modified for optimal efficacy. In a study by Jaruchalermrat and Niamlang (2021) a drug delivery hydrogel patch was developed using corn starch and controlled using an electric field. It was investigated for the treatment of hypertension and used hydrochlorothiazide (HCTZ) as a model drug showing a direct relation between the amount of HCTZ and electrical voltage.

To prevent the use of calcium propionate, which leads to the induction of diabetes mellitus through propionic acid, Ju *et al.* (2019) encapsulated essential oils that work against spoilage organisms using porous corn starch and to further preserve bread. The shelf-life was successfully extended and showed practical application potential in the baking industry. As an alternative to drugs for diabetes mellitus, algae usage has been studied. Fucoxanthin, a microalgae, has many useful medicinal properties such as anti-diabetic, antioxidant activity, anticancer, etc. but has limitations as a functional food. Porous starch was used to encapsulate fucoxanthin together with halloysite nanotube. The study concluded that porous starch and halloysite nanotube may be suitable as a carrier for encapsulation of bioactive compounds with low water solubility in functional food. Double encapsulation may be applicable for controlled or target release bioactive compounds (Oliyaei *et al.*, 2020).

In terms of medical applications, the use of porous starch-hydroxyapatite (HA) composites have shown positive results in bone regeneration. The clinical trial indicated that the Thai rice starch blend with cow bone are biocompatible and safe for bone regeneration, and also fully healed bones on neurological and orthopaedic patients (Punyanitya *et al.*, 2017). Studies also investigated the hematic effects of tranexamic acid-loaded porous starch (TAPS) with results showing TAPS to be successful in sealing injuries for homeostasis without any side effects. The powder had beneficial properties such as security, absorbability, affordable and easy production process (Xi *et al.*, 2018). There have been limited studies of cancer with porous starch but some have shown that porous starch may be used to encapsulate, increase the adsorption and dissolution rate of chemotherapeutic drugs.

Porous maize starch was used to deliver the anticancer drug doxorubicin using pectin/ chitosan beads and showed that most of the loaded drug was delivered to the colon proving to be an effective target-specific delivery system. It also showed that oxidation-prone or low solubility drugs could be delivered using this system (Zhu *et al.* 2019). Ning *et al.* (2018) conducted a study demonstrating an injectable hydrogel for encapsulation of an anti-cancer drug and specific drug delivery that is pharmaceutical grade. Micro porous starch was used to increase the anti-tumour activity showing injectable hydrogel with lysozyme to be suitable for anti-cancer drug delivery system.

2.10. Hyacinth bean (*Lablab purpureus*)

2.10.1. History, Agricultural and Geographical information

Hyacinth bean, scientifically known as *Lablab purpureus* and Dolichos lablab, belongs to the *Fabaceae* family. Origins of the hyacinth bean have not been identified but it is commonly found in Africa, Asia and the Americas (Kilonzi *et al.*, 2017). It can grow annually or for short periods, growing up to 6 m, twining, trailing, climbing or upright. Leaves are usually trifoliate and alternate with leaflets being rhomboid in shape. Flowers vary in colour, from either blue, purple or white and are approximately 1.5 cm long. The fruit of hyacinth bean are long and straight, approximately 4-15 cm long and 1-4 cm in width, smooth pods that contain up to 8 seeds. The seeds/ beans are oval and vary in colour from white to dark brown or black (Figure 2.8), depending on the cultivar (Al-Snafi and Esmail, 2017, Heuzé *et al.*, 2016,).

In India, the legume remains unexploited due to low productivity, prolonged growth rate, erratic growth and photosensitivity (Verma *et al.*, 2014). The hyacinth bean is drought tolerant, usually rain-fed and can withstand temperatures of 20-35°C (Akpapunam, 1996, Maass *et al.*, 2010). The legume crop can grow in areas with an annual rainfall of 60-90 cm. The occurrence and potential use of hyacinth bean in Africa has been studied by Maass *et al.* (2010), shown in Figure 2.9, is based on various species by applying FloraMap®.

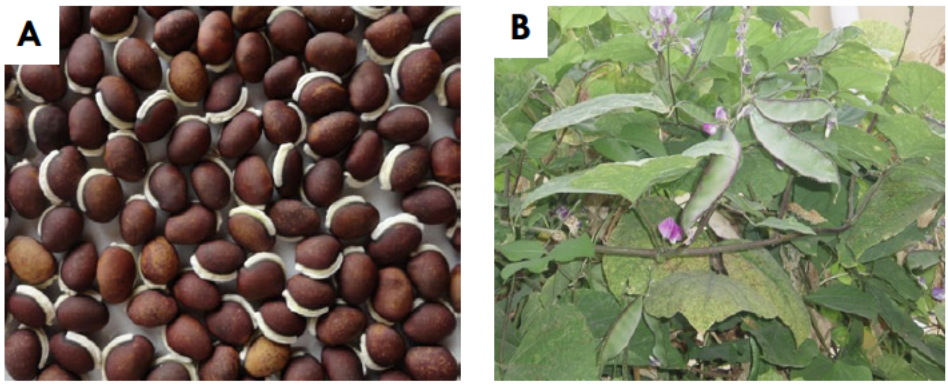

Figure 2.8: Hyacinth bean seeds (A) and pods (B) (Heuzé *et al.*, 2016).

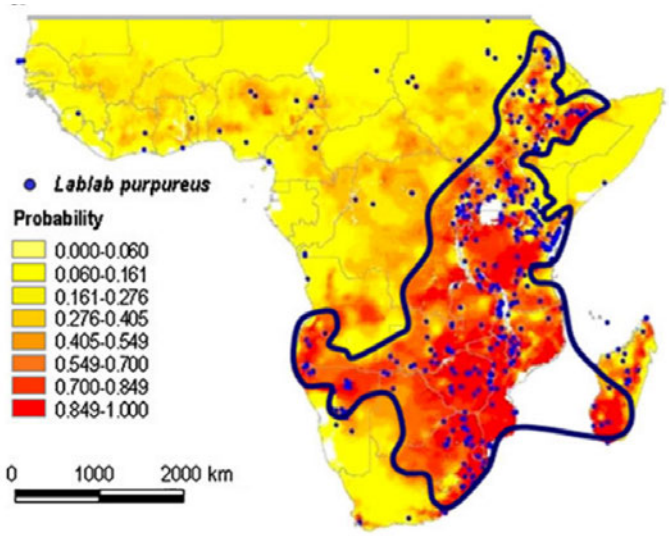

Figure 2.9: The potential of hyacinth bean being grown in Africa (Maass *et al*. 2010).

2.10.2. Uses of hyacinth bean

Low-income groups take advantage of the hyacinth bean as a relatively cheap source of protein. Reports have shown that the legume is versatile and the whole plant can be used for many purposes. The unripe pods and leaves are popular in parts of India as vegetables and the dried seeds as dhal (Verma *et al*., 2014). The beans are often prepared by soaking, de-hulling, boiling and ground into a paste which is fried. The hyacinth bean also has the potential to be used as animal feed due to the nutritional quality of the seed, stem, pod, leaf and root, which would benefit goats, pigs and cattle as well as horses, if supplemented with oats (Akpapunam, 1996). The hyacinth bean has shown various pharmacological properties such as anti-inflammatory, antimicrobial, anticancer, etc. (Al-Snafi and Esmail, 2017).

Traditionally the hyacinth bean plant was used as a remedy for alcohol intoxication, as well as for treatments against diarrhoea, gonorrhoea, nausea, cholera, etc. The pods were crushed and made into a juice for application for worm removal from inflamed ears and throats, as well as used to aid digestion. The flowers from the hyacinth bean were also used as a treatment for an inflamed uterus and to increase menstrual flow (Al-Snafi and Esmail, 2017).

2.10.3. Nutritional value of hyacinth bean

Generally, legumes are high in protein. This is evident in the hyacinth bean with protein levels ranging from 21.5-24.9%. They also have an adequate amino acid profile limiting in sulphur-containing amino acids, which is common in many legumes. They are high in carbohydrates (60.1%), crude fibre (6.8%), phosphorous and potassium (Akpapunam, 1996).

Studies on the approximate composition of leguminous foods revealed that they included 60-66% carbohydrates, 20-25% crude protein, 4.9-6.9% total dietary fibre, 2.6-4.1% crude fat, and 3.9-4.4% ash. Sodium, calcium, potassium, magnesium, iron, manganese, and phosphorus are among the minerals which are also present in the hyacinth bean together with niacin and ascorbic acid as examples of vitamins. All of the necessary amino acids, apart from those containing sulphur and tryptophan, are present in the seed protein. According to a study by Manickavasagan and Thirunathan (2020) hyacinth bean fatty acid makeup consists of 24% saturated fatty acids, 18% monounsaturated fatty acids, 57% polyunsaturated fatty acids, and 44% linoleic acids. Other research has shown that the dried seed has a 33% starch content as its main constituent, 25% protein, a very low fat level of 0.8%, and a high 7.2% dietary fibre content.

Raffinose and stachyose, both 3.5% oligosaccharides, were also present, as well as phytic acid, 82.0 mg/g, phosphorus, 430 mg/g, and phytates, 243 mg/g. The leaves included up to 28% protein, legumes, 155 mg of iron, and 30 mg of zinc per 100 g of dry weight. The grain had 57 mg of iron and 34 mg of zinc per kilogramme. The content of the ripe seeds varied significantly, though. According to Al-Snafi and Esmail (2017) percentages of crude protein, crude fibre, and total carbohydrates ranged from 22.4-31.3% and 54.2-63.3%, respectively.

2.10.4. Hyacinth bean starch

With respect to cultivar, cultivation techniques, and plant growth conditions, the amylose concentration of the starch from legumes can range from 17.0-51.69%. Additionally, iodine, fatty acids, and monoglycerides combine with amylose to produce helical clathrate inclusion complexes. It is generally accepted that it results from a transformation of the amylose coil conformation to helix shape. It is known that the guest molecules penetrate the amylose helices' core cavities, reducing their availability in free form.

Due to the use of various estimating approaches, under- or overestimation is therefore likely to occur. The amylose content may affect the starch physicochemical and functional characteristics, including its tendency to gelatinize, swell, paste, and retrograde (Wani *et al.*, 2016). According to its digestibility, rate and duration of glycaemic response, starch and high starch dietary items can be categorised (Singh *et al.*, 2010).

The starch content of hyacinth seeds range from 13.2-15.8%, according to a research characterising the starch from three kinds of *Lablab purpureus*. The Rongai brown hyacinth bean cultivar has the largest percentage of tiny granules, with granule sizes ranging from 12.51-20.56 μm. The starch crystallinity levels ranged from 37.0-46.3%, and their diffraction patterns were of the C-type. The amylose contents, both apparent and definitive; were 23.1-26.0% and 17.5-23.6%, respectively. The starches also exhibited high gelatinization initiation temperatures (To = 73.5-75.7°C), one-phase swelling, and amylose leaching patterns. The starch pastes had considerable shear thinning, poor clarity, and poor freeze-thaw stability, according to Nwokocha *et al.* (2010).

2.11. Aim and Objectives

Research problem

Current cancer treatments often lead to the destruction of healthy cells and escalated toxicity, therefore a novel treatment that is non-toxic, efficient and inexpensive is required. Embedding silver nanoparticles into porous starch may provide a suitable oral delivery system against cancer.

Aim

To develop a novel delivery system for silver nanoparticles using porous starch to target cancer cells (CACO, MCF-7 and C2C12).

Objectives

1. To isolate and characterize porous starch (SEM, FTIR, XRD, DSC, *in vitro* starch digestibility, and physicochemical properties) from *Lablab purpureus* by hydrolysis, freeze-thaw and solvent-exchange.
2. To synthesize and characterize silver nanoparticles embedded in porous starch (UV-VIS, TEM, particle size analysis, zeta-potential, FTIR, XRD)
3. To determine the efficacy of silver nanoparticles embedded in porous starch against cervical cancer (HELA), colon cancer (CACO), breast cancer (MCF-7), and muscle (C2C12) cell lines using the MTT assay.

Chapter 3: Structural and physicochemical characterization of porous starch prepared by enzymatic hydrolysis, solvent-exchange, and freeze-thaw cross-linking treatments

Abstract

Porous starches have been researched for its applications of its characteristics for use in various industries. Although, it has been noted that different methods are used to influence the properties manifested. In this study, native starch (NS) isolated from hyacinth bean (*Lablab purpureus*) was used to create porous starch using three different methods *viz*. solvent-exchange (SE), enzyme hydrolysis (EH) and addition of mercaptosuccinic acid known as freeze-thaw (FT). The structural characteristics (Fourier-transform infrared spectroscopy, X-Ray Diffraction) of SE and EH were very similar to that of NS. The gelatinization properties of the porous starches were higher (97.15-112.86°C) than NS (93.00-103.69°C). The pasting properties of SE and EH were higher than NS, whilst FT did not pose any pasting abilities. This was due to its high solubility (42.92±1.70 %) and lipophilic nature (4.63±0.42 g/g). The adsorption properties of SE (4.06-16.35 mg/g) and EH (4.31-15.45 mg/g) were similar to NS (3.53-15.50 mg/g). The swelling power of SE (9.16±0.19 %) and EH (9.25±0.13 %) were similar to NS (9.76±0.43 %), whilst the amylose contents (15.48-19.43 %) were lower than NS (20.68±4.39 %). Only the SE (11.42±3.40 %) from the porous starches had resistant starch present, whilst EH had mostly rapidly digestible (13.23±0.00 %) and slowly digestible starch (127.16±0.00 %). These structural and physicochemical characteristics showed that these porous starches may be suitable in delivery systems, improving solubility of drugs and adsorbing dyes.

Keywords

Porous starch, delivery system, encapsulation, starch

3.1. Introduction

The most prolific carbohydrate in the human diet is starch, with starch granules usually 1 µm to over 100 µm in diameter, oval in shape, but can occur as spherical, circular, elliptical, and irregularly shaped (Hoover *et al.*, 2010). Granular starch can be found in most parts of higher plants and consists of amylose and amylopectin. Amylose is a linear molecule, makes up 20-30% of starch, and is made by α-(1-4)-glycoside bonding of D-glucose units. The amylose content may have an impact on the functional and physicochemical properties of the starch such as gelatinization, swelling, pasting, and retrogradation behaviour (Wani *et al.*, 2016). Amylopectin is a large branched molecule, making up about 70-80% of starch, consisting of linear chains α-(1-4)-linked D-glucose units interconnected through α-(1-6) glycosidic bonds (Hanafi, 2020). The structure of starch is presented in amorphous and crystalline parts forming a unique semi-crystalline pattern. C-type crystalline patterns are found in legume starches and are a combination of A and B- type patterns. The main differences of these structural patterns are the crystal packing and water content (Rostamabadi *et al.*, 2019).

Legumes have more slowly digestible starch than cereals and tubers and have been used for many medicinal purposes (Phillips, 1993). Legume starch is an excellent source of dietary fibre and due to the presence of resistant starch exhibit a low glycaemic index. Legumes have up to 10% higher amylose starch content than cereals except for high amylose cereal starches (Tayade *et al.*, 2019). Hyacinth bean (*Lablab purpureus*) is a versatile drought tolerant legume grown predominantly in Asia and Africa (Kokila *et al.*, 2014, Naeem *et al.*, 2020). Hyacinth bean flour has been shown to have mostly starch (48.66-51.02%) and protein (27.35-29.47%) (Naiker *et al.*, 2020). Hyacinth bean has also shown to be an excellent source of essential amino acids and fatty acids, tocopherols, bioactive components and carotenoids (Habib *et al.*, 2017). Although native starch has many desirable characteristics that are useful to the food and pharmaceutical industries, there are also limitations such as its sensitivity to processes such as extreme temperature, low pH, high shear rate, and freeze-thaw variation. Modification of native starch to include pores have been noted to improve many starch characteristics some of which are: water binding capacity and solubility, granularity, gelatinization temperature, paste viscosity, etc. (Chen *et al.*, 2020; Sujka *et al.*, 2018).

Porous starch has many desirable properties such as an enhanced adsorption capacity which is highly desired in drug loading applications to improve the bioavailability of drugs that are typically insoluble by increasing the drug dissolution. Due to the capacity for high drug loading, being inert, bio-adhesive, biocompatible, and comfortable for the patient, porous starch is an ideal material for a drug delivery system. Other improved characteristics are its large specific surface area and encapsulating properties (Wang *et al.*, 2019). Methods used to produce porous starch are usually physical, chemical, and/or enzymatic, with more commonly reported methods being solvent-exchange, enzyme hydrolysis and ultrasound. The technique is often chosen with consideration to specified pore size, pore volume, specific surface area and optimized production output. Porous starch may be characterized by its structure and physicochemical properties where structural analysis shows pore size, shape, crystallinity, and intermolecular bonds. Whereas, adsorption properties, swelling power and solubility, rheological, pasting and thermal properties may be determined by physicochemical analysis (Chen *et al.* 2020, Sujka *et al.* 2018).

Notable uses of porous starch have been carriers for medication, encapsulation of dietary supplements and adsorbents for pollutants. Biocompatibility, non-toxic and biodegradable abilities of porous starch are advantageous for encapsulation and slow-release of food ingredients. Encapsulation has also been used to create stability of food ingredients. These abilities have also been utilized in the pharmaceutical and environmental industries. Porous starch may be used in the production of controlled-release drug delivery and adsorption of various detergents. Before allocating a use for porous starch, the influence of the production technique of its properties should be investigated. Therefore, this study involves the production and characterization of porous starches using three techniques viz. solvent-exchange, enzyme hydrolysis and freeze-thaw (addition of MSA) (Chen *et al.* 2020, Sujka *et al.* 2018).

3.2. Materials and methods

3.2.1. Sample preparation

Hyacinth bean (*Lablab purpureus*) samples were obtained from the Reservoir Hills, Umgeni River Valley (KZN), South Africa, with a herbarium voucher containing specimen deposited in the Ward Herbarium (UDW), University of KwaZulu-Natal, Westville Campus, Durban. All chemicals used were of reagent grade purchased from Sigma-Aldrich.

Flour preparation

The hyacinth bean seeds were soaked overnight in 10% (w/v) sodium hydroxide, de-hulled and then oven dried at 50°C for 24 h. The dried seeds were milled [Alpine Fine impact mill (Hosokawa Alpine AG, Augsburg, Germany)] into flour and sieved (180 µm). The flour was then defatted using hexane (1:5, w/v) overnight at 200 rpm (Stuart Orbital Shaker SSL 1, Stuart Equipment) and centrifuged at 10 000 × *g* for 20 min at 20°C (Heareus multifuge × 3 FR centrifuge, Thermo Scientific). The hexane was decanted, the flour air-dried in a fume hood for 24 h and stored at 4°C until required (Mohan and Mellem, 2020).

Starch isolation

The starch was isolated from the defatted flour using the method described by Rengadu *et al*. (2020). The flour was diluted in 0.025 $molL^{-1}$ Na_2SO_3 (1:10, w/v). The mixture was then homogenized and left at room temperature for 1 h. The slurry was then centrifuged at 5 000 × *g* for 15 min, washed with ethanol twice, and then the pellet was washed with distilled water, dried and stored in 4°C until required. A portion of the starch was kept for native starch analyses.

3.2.2. Porous starch preparation

Enzyme hydrolysis

Starch was immersed in sodium acetate buffer (pH 4.6, 25% w/v) and stirred for 20 min at 150 rpm in a 40°C water bath. A mixture (1%, 1:4) of α-amylase (Sigma 86250; 1.5 U/mg) and amyloglucosidase (Sigma A7095; 260 U/mL) was added to the starch slurry. The mixture was left to agitate for 24 h in a 40°C water bath. The enzymes were inactivated by adding 20 mL of sodium hydroxide solution (4%, w/v) and centrifuged at 1 800 × *g* for 5 min. The pellet was washed with distilled water (3 times) and then freeze-dried (Guo *et al*., 2013).

Solvent-exchange

Porous starch was produced using the solvent-exchange method described by Wu *et al.* (2011). Briefly, 8% w/v of starch and water suspension was boiled for 30 min while stirring. The solution was cooled to 85°C and poured into centrifuge tubes. The slurry was chilled in a refrigerator (5°C) overnight to facilitate gelation and thereafter frozen (-10°C) overnight. The frozen starch was submerged in 95% ethanol for 24 h. The slurry was then rotary evaporated at 30°C to remove the ethanol and freeze-dried.

Freeze-thaw

Using the method described by Bao *et al.* (2016) mercaptosuccinic acid (MSA), was dissolved in Milli-Q water (5%, w/v) and starch added to the MSA solution (1:1). The mixture was then heated to 90°C and stirred for 30 min to form gelatinized composites of starch and MSA which were then freeze-dried.

3.2.3. Characterization of porous starch

Fourier-transform infrared spectroscopy (FTIR) analysis

The chemical structure of the porous starch was determined using an FTIR spectrophotometer (Cary 630, Agilent, CA, USA). The spectrum range was 650-4 000 cm^{-1}.

X-ray diffraction (XRD) analysis

The XRD measurements for the starch samples were taken using a X-ray diffractometer (D8 Advance, BRUKER AXS, Germany) with Cu Kα radiation ($\lambda K\alpha_1$ = 1.54056Å) at a voltage of 40 kV and current of 40 mA. The scan range was between 0° and 80° with the change rate of 0.5°/min in 2θ.

Differential scanning calorimetry (DSC) analysis

The gelatinization temperatures of the samples were determined using a Differential Scanning Calorimeter (DSC 25, TA instruments, New Castle, USA). Starch and distilled water were added (1:2, w/v) and sealed in a hermetically stainless-steel crucible which were left at 4°C overnight to equilibrate. The samples were then heated at 10°C/min and scanned between 30-120°C. An empty stainless-steel crucible was used as a blank control (Wu *et al.*, 2020).

3.2.4. Total starch determination and *in vitro* digestibility

Total starch was determined using a commercially available kit (GOPOD kit) and following the supplier's instructions (Megazyme International Ireland Ltd., Bray Business Park, Bray, Co. Wicklow, Ireland). Briefly, 5 mL of 80% ethanol was added to 100 mg of sample and incubated at 85°C for 5 min. The wet samples were vortexed, thereafter 5 mL of 80% ethanol was added. The mixture was then centrifuged for 10 min at 3 000 × *g*. The supernatant was removed, and 2 mL of 2 molL^{-1} KOH added. The samples were stirred in an ice water bath for 20 min, subsequently 8 mL of 1.2 molL^{-1} sodium acetate buffer (pH 3.8) was added and agitated lightly. The enzyme mixture of 70 mg of α-amylase (Sigma 86250; 1.5 U/mg) and 78 µL of amyloglucosidase (Sigma A7095; 260 U/mL) was added. The solutions were mixed well and then incubated for 30 min at 50°C. After centrifuging for 10 min at 3 000 × *g*, 33 µL were transferred to test tubes and 3 mL of the GOPOD reagent added. The tubes were incubated for 20 min at 50°C, thereafter the absorbance was measured at 510 nm.

In vitro starch digestibility was determined using the method described by Naiker *et al.* (2020) with minor modifications. In brief, 500 mg of sample was stirred in 1 mL of porcine α-amylase (Sigma 86250; 1.5 U/mg of carbonate buffer pH 7). Then, 5 mL of pepsin (Sigma P-6887) solution prepared in 0.02 molL^{-1} HCl was added and incubated at 37°C for 30 min. The digesta was neutralized with 5 mL of 0.02 molL^{-1} NaOH, and further adjusted with 25 mL of 0.20 molL^{-1} sodium acetate buffer pH 6, with a pancreatin (Sigma P-1750; 2 mg/mL of acetate buffer) and amyloglucosidase (Sigma A7095; 260 U/mL of acetate buffer) mixture. Starch digestibility (%) was determined by quantification of glucose in the digesta between 0 and 180 min of digestion using the Megazyme GOPOD kit. The factor conversion from glucose to starch content used was 0.90. Determination of rapidly digestible starch (RDS), slowly digestible starch (SDS), and resistant starch (RS): RDS and SDS were measured as the percentage of total starch digested (%) at 20 and 120 min of enzymatic digestion respectively. Resistant starch was measured as the difference between the total starch and the sum of RDS and SDS contents for respective samples.

3.2.5. Amylose content

The amylose content of the starches was determined using the method described by Kaufman *et al*. (2015). Briefly, 5 mg of sample was weighed and added with 1 mL of 90% DMSO to a 2 mL Eppendorf tube, heated at 95°C and vortexed every 5 min for 1 h. The sample was then cooled and 100 µL was decanted into a 96-well plate. A solution of 100 µL of 90% DMSO and 3.04 g/L iodine solution was added. The plate was then shaken for 2 min and 20 µL was removed and placed into a new 96-well plate. Thereafter, 180 µL of distilled water was added. The plate was shaken for 2 min before reading the absorbance at 510 and 620 nm. The blank included 180 µL of distilled water, 20 µL of the 90% DMSO, 100 µL of 90% DMSO and 3.04 g/L iodine solution.

3.2.6. Swelling power and solubility

The method described by Ramsookmohan *et al*. (2020) with modifications was used to determine the swelling power and solubility index of the starches. Briefly, samples (2% m/v) were incubated in a water bath for 30 min at 85°C and mixed after every 5 min. After cooling to room temperature, the samples were centrifuged at 5 000 × *g* for 15 min. The pellet was weighed, and the supernatant poured into petri plates and dried overnight. The swelling power was determined by the ratio of the pellet and initial mass and the solubility (g/g) was determined by the gain in weight of the supernatant compared to the initial mass.

3.2.7. Pasting

The pasting properties of starches were determined using a Rapid Visco™ Analyzer (Perten Instruments Australia). Approximately 2 g of starch (corrected to 14% moisture basis) as well as 25 mL of distilled water were combined and stirred in the aluminum RVA sample canister. The samples were heated to 50°C and stirred at 960 rpm for 10 s. The speed was decreased to 160 rpm for 50 s. The temp was then increased to 95°C before decreasing to 50°C at 11 min. The test duration was 13 min with the viscosity recorded in RVU (rapid viscosity units).

3.2.8. Water, oil and pigment adsorption capacity

The water, oil and pigment adsorption capacities were determined using the method described by Guo *et al*. (2021). Starch was diluted in distilled water/ canola oil (1%, m/v) and stirred for 25 min. The solution was filtered, and the filter paper weighed.

The adsorption capacities (%) were determined by dividing the mass of starch adsorbing water/oil by the sample mass. For the pigment adsorption, methylene blue (20 mg/L) was added to the starch (1% m/v) samples and then stirred for 90 min. The absorbance was measured at 660 nm. Equation 1 was used to determine the pigment adsorption capacity (PAC).

$$PAC = (c1 - c2) \times v \times \frac{m}{w} \quad \text{.....[1]}$$

Where $c1$ is pigment content in a solution before adsorption; $c2$ is pigment content in a solution after adsorption; v is pigment solution volume; w is dry sample weight; m is pigment molecular mass.

3.2.9. Statistical analysis

Most tests were carried out in triplicate and reported as mean $\pm$ standard deviation with a one-way analysis of variance (ANOVA) and a Tukey post-hoc test was used to determine statistical differences. *In vitro* starch digestibility and amylose content tests were done in duplicate, and a two-way analysis of variance was used to determine the statistical differences. All statistical analyses were performed using GraphPad Prism version 5.01 for Windows (GraphPad Software, San Diego California USA).

3.3. Results and Discussion

3.3.1. Preparation and characterization of porous starch

The aim of the study was to create porous starches that had improved characteristics compared to native starch and to document the effects. The solvent-exchange method involved the gelatinization of the starch and then the displacement of the water with ethanol to form an alcogel, thereby producing a foam (Wu *et al*. 2011). In the freeze-thaw method, a xerogel was produced with the addition of mercaptosuccinic acid (MSA). The addition of the MSA during gelatinization of the starch allows for the insertion of the MSA into the starch chains (Bao *et al*. 2016). Enzyme hydrolysis produced porous starch that was partially hydrolyzed by α–amylase and amyloglucosidase to modify the granule structural integrity and surface characteristics (Guo *et al*., 2013, Whistler *et al*., 2012).

The characteristic chemical bonds and functional groups that influence the structural organization of the native starch (NS) and porous starch samples, were identified using Fourier-Transform Infrared spectroscopy (Figure 3.1). The solvent-exchange (SE) and enzyme hydrolysis (EH) bands were not significantly different from the NS band. The absorption peaks at the O-H stretch for NS, SE and EH were between 3276.33 and 3265.15 cm^{-1}, whilst the porous starch produced using the freeze-thaw (FT) method did not have a peak present. These wide peaks are characteristic of vibration stretching of hydroxyl groups showing weak intramolecular alcohol bonds. The reduced intensities of the porous starches compared to the intensities of NS, indicates the formation of pores which decreased the density of the granule. Absorption peaks between 2907.32 and 2925.96 cm^{-1} are indicative of C-H stretching and medium strength alkane bonds.

The peak at 1 684.74 cm^{-1} on the FT band represent strong, conjugated ketone bonds at C=O stretching, whilst the peaks at 1 636.30 and 1 643.76 cm^{-1} of SE, EH and NS spectra represents strong, alkene bonds at C=C stretching (Dıblan *et al.*, 2018). All starches had bands at 1 077.20 and 991.47 cm^{-1} which is characteristic of strong C-O stretching, C=C bending. The FT band had a peak at 767.83 cm^{-1} showing strong, tri-substituted C-H bending. The similarity amongst the vibration bands of the porous starches are indicative of similar chemical structures, although the change in intensities show the presence of holes (Ghavimi *et al.*, 2015). The porous starch produced by FT has a band significantly different from native starch which may be attributed to the presence of mercaptosuccinic acid (Bao *et al.* 2016).

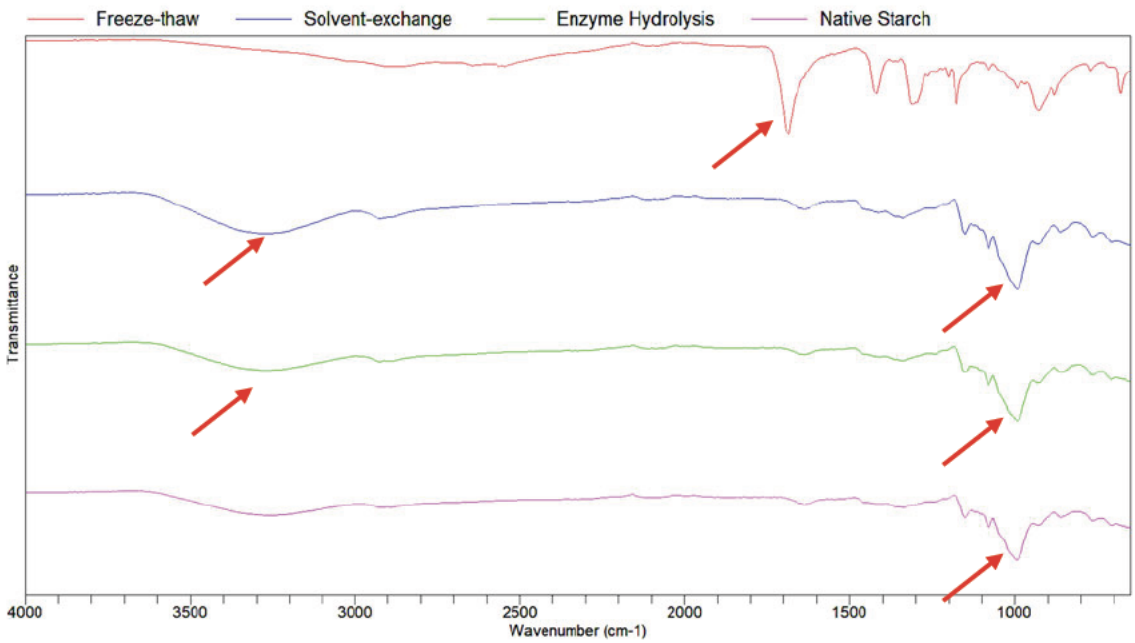

Figure 3.1: FTIR spectra of porous and native starch samples from *Lablab purpureus*.

The crystalline patterns and arrangement of the starch granule structure is determined using x-ray diffraction (Figure 3.2). The diffractograms of NS and the porous starch samples have three distinct peaks around (2θ) values 15°, 17°, 18° and 22°. Peaks at these angles are characteristic of both A- and B-type crystalline patterns which indicates a C-type crystalline pattern typically found in legumes (Chen, 2021, Bajaj *et al*., 2018). The SE and EH porous starch samples are very similar to the diffractogram of NS with only slightly lower intensities after 30°. FT had almost no similarities to NS with a low intensity which may be due to a very weak crystalline region and highly hydrolysed starch, through treatment by mercaptosuccinic acid (Bao *et al*. 2016).

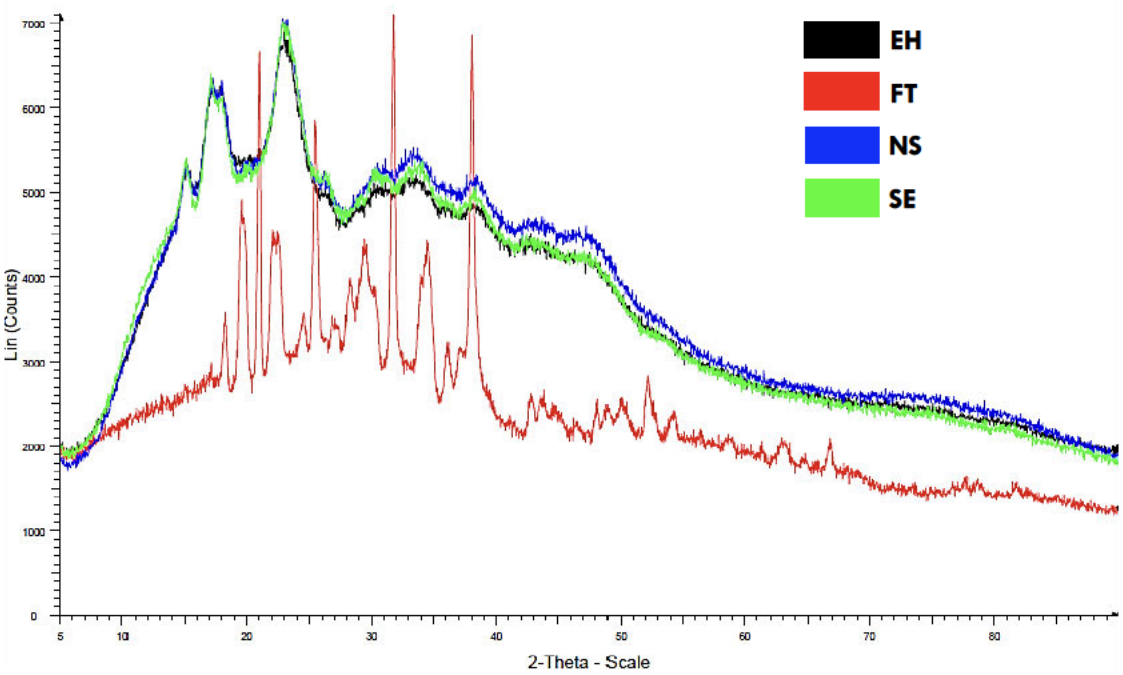

Figure 3.2: XRD patterns for porous and native starch samples from *Lablab purpureus*. [NS: native starch; EH: enzyme hydrolysis; SE: solvent-exchange; FT: freeze-thaw]

Table 3.1: Enthalpies from phase changes for *Lablab purpureus* porous starch samples (dwb)

Sample	T_o (°C)	T_p (°C)	ΔH (J/g)	T_c (°C)	ΔT_{gel} (°C)
NS	93.00±13.78^a	102.66±0.45^a	102.36±4.81^a	103.69±3.26^a	12.05±15.12^a
SE	105.33±6.00^a	113.08±0.38^a	111.12±4.90^a	112.86±0.84^a	7.53±5.16^a
EH	97.15±0.50^a	108.58±1.31^a	112.24±0.37^a	101.95±2.31^a	4.80±1.82^a
FT	106.10±1.73^a	105.09±0.39^a	103.35±4.29^a	108.84±1.63^a	2.74±0.10^a

All data is expressed as mean±standard deviation (n= 3). Values with different superscript letters are significantly different ($p<0.05$). [NS: native starch; EH: enzyme hydrolysis; SE: solvent-exchange; FT: freeze-thaw; ΔH: enthalpy of gelatinisation; ΔT_{gel}: gelatinisation temperature range ($T_c - T_o$); T_o: onset temperature; Tp: peak temperature; Tc: conclusion temperature]

The gelatinization properties of NS and porous starch are represented in Table 3.1 and were evaluated using Differential Scanning Calorimetry (DSC). The transition (T_o, T_p, T_c) temperatures of the porous starch samples (97.15-112.86°C) are higher than that of NS (93.00-103.69°C) but not significantly different. During gelatinization, the double helix crystalline nature of starch is unwound, and it becomes amorphous due to the loss of the maltese cross. The enthalpy of gelatinisation (ΔH) of the porous starches (103.35-112.24°C) are higher than the enthalpy of NS (102.36°C).

This may be due to the increase in temperature breaking the double helix structure and hydrogen bonds, therefore, more energy is required (Lacerda *et al.*, 2018, Zhao *et al.*, 2018). The gelatinisation temperature range (ΔT_{gel}) was the highest for NS showing its heterogeneity in its granule crystalline regions (Acevedo *et al.*, 2019). The pasting properties of the native and porous starches are shown in Figure 3.3 and was determined by the heating-cooling cycle using a rapid visco-analyser. The peak viscosities of SE (2 392.00 RVU) and EH (2 508.00 RVU) was higher than the peak viscosity of NS (1 896.00 RVU) whilst the peak viscosity of FT was 168.00 RVU. This may be due to the presence of pores which increase the shear force when heated since the disrupted starch granules are more susceptible to breakage (Chen *et al.*, 2020). The FT sample did not form a paste. This may be due to the presence of the mercaptosuccinic acid. The setback was the highest for EH at 12 530.00 RVU, followed by SE at 876.00 RVU and then NS at 727.00 RVU while FT had a setback value of 13.

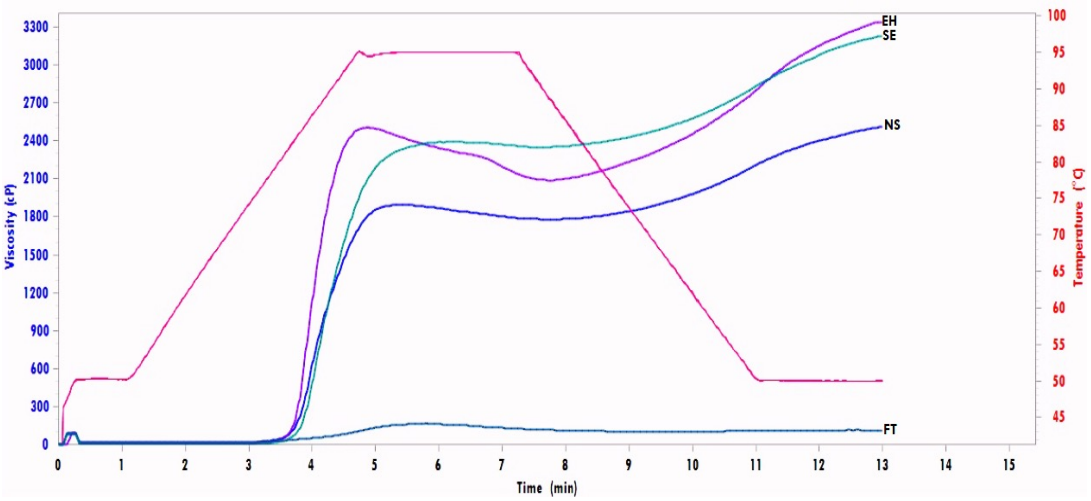

Figure 3.3: Pasting properties of porous and native starch samples from *Lablab purpureus*. [NS: native starch; EH: enzyme hydrolysis; SE: solvent-exchange; FT: freeze-thaw]

The setback values (the area between the peak and final viscosity) show the ability of the fractional amylose chains reforming a helical structure. The amylose chains of the porous starch samples (SE and EH) had higher retrogradation abilities than NS. The granule size may have an influence on the pasting properties and the difference in the pasting curves may be due to the method of production of the porous starch (Bajaj *et al.*, 2018). Similar curves were produced in a study by Dura *et al.* (2014) when porous starch was produced using α-amylase and amyloglucosidase under various pH conditions (pH 4-6).

3.3.2. Physicochemical properties

The amylose content and amylopectin branch chains influence the amorphous and crystalline natures of starch (Lacerda *et al.*, 2018). The amylose content also influences various characteristics of starch such as: maintaining the granule integrity, reducing the swelling power and solubility of starch and preventing gelatinization (Chen *et al.*, 2019). The amylose content was determined using the equation obtained from the standard curve. The amylose content of the porous starch samples (0.00-19.43%) were lower than the amylose content of the NS (20.68%). The FT sample was significantly different from NS, EH and SE (Table 3.2).

This indicates that the amylose was preferentially hydrolysed by each treatment. The type and combination of enzymes greatly influence the level of amylose hydrolysis and the combined use of α-amylase and amyloglucosidase may have resulted in the hydrolysis of the amorphous and crystalline regions of the starches (Benavent-Gil and Rosell, 2017a).

As seen in Table 3.2, the amylose content of NS (20.68) coincided with the results reported for various legumes 20-23% (Chavez-Murillo *et al.*, 2018) and was higher than the amylose content of native pea starch (13.12-16.34%) (Gao *et al.*, 2022). Total starch of all the samples were significantly different. Solvent-exchange (77.03%) and EH (76.09%) had higher starch levels than NS (72.42%), whilst FT (40.60%) had lower starch levels than NS. The resistant starches were significantly different with SE (11.42%) having a lower percentage of resistant starch than NS (16.71%), whilst EH and FT did not have any resistant starch. The SDS (47.26-127.16%) and RDS (8.46-13.23%) values of SE, EH and NS were significantly different, whilst FT was completely hydrolysed at initial introduction of the enzymes used for *in vitro* starch digestibility (Figure 3.4). The method used to produce the porous starch, number and size of the pores in porous starches may be influential in the digestibility of the starch (Benavent-Gil and Rosell, 2017b)

Table 3.2: Amylose content and *in vitro* starch properties of porous starch samples for *Lablab purpureus*

Sample	Amylose content (%)	TS (%)	RS (%)	SDS (%)	RDS (%)
NS	20.68±4.39^{a}	72.42±0.04^{a}	16.71±1.46^{a}	47.26±0.70^{a}	8.46±0.70^{a}
SE	19.43±3.46^{a}	77.03±0.01^{b}	11.42±0.00^{b}	52.68±0.00^{b}	12.92±0.00^{b}
EH	15.48±3.40^{a}	76.09±0.01^{c}	0.00±0.00^{cd}	127.16±0.00^{c}	13.23±0.00^{bc}
FT	0.00±0.00^{b}	40.60±0.04^{d}	0.00±0.00^{d}	0.00±0.00^{d}	0.00±0.00^{d}

All data is expressed as mean±standard deviation (n= 3). Values with different superscript letters are significantly different ($p<0.05$). [NS: native starch; EH: enzyme hydrolysis; SE: solvent-exchange; FT: freeze-thaw; TS: total starch; RS: Resistant Starch; SDS: Slowly Digestible Starch; RDS: Rapidly Digestible Starch]

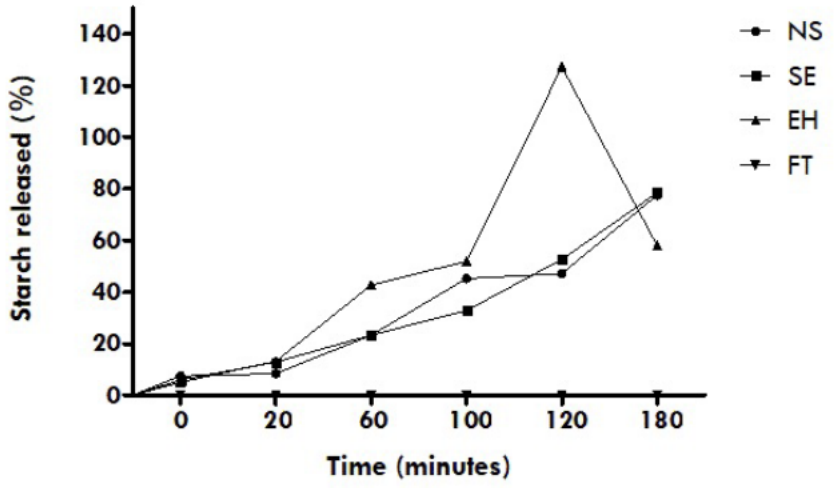

Figure 3.4: *In vitro* starch digestion of porous and native starch samples from *Lablab purpureus*. [NS: native starch; EH: enzyme hydrolysis; SE: solvent-exchange; FT: freeze-thaw]

The WAC and OAC were determined by the amount of water/oil adsorbed (Table 3.3). The water adsorption capacity of the porous starches (5.42-6.20g/g) were not significantly different from NS (5.75 g/g) whereas the oil adsorption capacity of the porous starches (4.06-4.63 g/g) was significantly different from NS (3.53 g/g). It had been shown that potato porous starch modified with mercaptosuccinic acid was successful in removing Gardenia Yellow, but was expensive to produce due to the cost of mercaptosuccinic acid (Bao *et al.* 2016). Enzyme hydrolysis had the highest WAC and FT had the highest OAC. The adsorption capacities of the NS and porous starch samples (3.53-6.20 mg/g) were higher than those reported for wheat (0.65-1.10 mg/g), rice (0.92-1.16 mg/g), potato (0.48-1.20 mg/g) and cassava (0.63-1.13 mg/g) starch

(Benavent-Gil and Rosell, 2017a). The higher WAC suggests that hyacinth bean starch has a more hydrophilic than lipophilic nature (Chen *et al*. 2019). The PAC was not significantly different for EH (15.45 mg/g) and NS (15.50 mg/g) whilst SE (16.35 mg/g) had the highest PAC. The results for the hyacinth bean porous starch and NS (13.85-16.35 mg/g) was higher than adsorption capacities for methylene blue of native corn starch (3.11 mg/g) and cross-linked porous corn starch (7.26 mg/g) as well as porous starch obtained by SE (0.43-0.58 mg/g) (Guo *et al*. 2013; Oliyaei *et al*. 2020).

The swelling powers for EH and SE (9.16 %, 9.25 %) were not significantly different from NS (9.76 %) whilst FT was significantly different (3.47 %). The solubility of the EH and SE (3.22%, 4.08%) samples were higher than that of NS (2.44 %) but FT (42.92%) was significantly higher. *Amaranthus cruentus* had lower swelling and solubility properties (0.00-7.26%) than results from *Lablab purpureus* shown (Ramsookmohan *et al*. 2020). Similar swelling powers were reported by Zhang *et al*. (2019) at 80°C for Red adzuki (6.87%) and Baiyue (6.84 %) legumes, whilst the solubility's were 9.50% and 7.33%, respectively. The swelling power and solubility may have been influenced by various properties such as amylose content, particle size distribution, surface area, water adsorption capacity and crystallinity (Rengadu *et al*. 2020). The low gelatinization and retrogradation properties shown in the DSC results of FT reflects in its low swelling power and high solubility results. The high swelling powers of the starches may also be related to the hydrophilic nature of hyacinth bean (Naiker *et al*. 2020).

Table 3.3: Physicochemical characteristics of native and porous starch samples for *Lablab purpureus*

Sample	WAC (g/g)	OAC (g/g)	PAC (mg/g)	SP (%)	Solubility (%)
NS	5.75±0.20^{a}	3.53±0.22^{a}	15.50±0.32^{a}	9.76±0.43^{a}	2.44±0.47^{a}
EH	6.20±0.28^{a}	4.31±0.14^{b}	15.45±0.13^{ad}	9.25±0.13^{a}	3.22±0.33^{a}
SE	5.42±0.42^{a}	4.06±0.06^{ab}	16.35±0.11^{b}	9.16±0.19^{a}	4.08±0.31^{a}
FT	5.58±0.41^{a}	4.63±0.42^{bc}	13.85±0.06^{c}	3.47±0.11^{b}	42.92±1.70^{b}

All data is expressed as mean±standard deviation (n= 3). Values with different superscript letters are significantly different ($p<0.05$). [NS: native starch; EH: enzyme hydrolysis; SE: solvent-exchange; FT: freeze-thaw; WAC: water adsorption capacity; OAC: oil adsorption capacity; PAC: pigment adsorption capacity; SP: swelling power]

3.4. Conclusion

The production method used to prepare porous starch greatly influences its structural and physicochemical properties. The structural and chemical natures of the porous starch samples produced, using SE and EH, were similar to that of NS, whilst the addition of MSA in the freeze-thaw method had greatly influenced its characteristics. The gelatinization property (DSC) of FT was lower than the SE and EH, therefore it would be useful for absorption of dyes due to its high solubility. Solvent-exchange and EH had more favourable results such as increased adsorption properties, swelling powers, pasting, and gelatinization properties, showing that they may be useful in carriers in delivery systems and increasing the adsorption of poorly soluble drugs. Further research on different preparation techniques, of developing porous starch with specific properties, is essential for its industrial commercialization.

Chapter 4: Anti-cancer potential of silver nanoparticles embedded in porous starch

Abstract

Using porous starch created by solvent exchange, silver nanoparticles were successfully created. They were then examined for *in vitro* cytotoxicity activity in CACO, MCF-7, and HELA cancer cells as well as C2C12 healthy cells. According to the features, porous starch contributed to the effective reduction and stability of the nanoparticles. The particle size distribution exhibited peaks at 18 769 and 16 226 nm, the zeta potential was -34.1 mV, the UV-vis spectra had a peak at 425 nm, the FTIR showed intensity bands at hydroxyl stretching, and the TEM indicated spherical nanoparticles. The nanoparticles demonstrated less cytotoxicity in the CACO and HELA cell lines, but more inhibition in the MCF-7 cell line than camptothecin. The overall cell viability for the C2C12 cell line was favourable for silver nanoparticles. Further research is required for optimizing the potential of the silver nanoparticles embedded in porous starch.

Keywords

Silver nanoparticles, cytotoxicity, porous starch

4.1. Introduction

Nanoscience has been significantly growing in application recently due to its range of metal-nanoparticles and the versatility of use within the food sector. Nanoparticles are particles that are 1-100 nm in size with silver nanoparticles most commonly used due to their unique physicochemical properties present. Nanoparticles are popular in many applications due to associated morphological properties, distribution, structure, size, and surface area. Currently chemistry, medicine, energy and electronics are the most common fields making use of metal nanoparticles on a global scale (Huy *et al*., 2020, Abdulsahib, 2021). With an emphasis on biomedicine for therapy against breast, stomach, and colon cancer, cytotoxicity, and *in vivo* and *in vitro* research of anti-inflammatory drug catalysts, silver nanoparticles have been employed in surgical tools, water treatments, electronics, bio-sensing, and other applications. Silver nanoparticles are regarded as non-toxic and eco-friendly in relatively low quantities and shows promise in developing efficient anticancer therapies (Abdulsahib 2021).

There are many techniques used to produce silver nanoparticles including, physical biological and chemical methods. However, chemical and physical techniques are expensive, complicated and toxic (Rajeshkumar and Bharath 2017). Biological methods make use of polysaccharides, microorganisms, and plant extracts as reducing agents, commonly referred to as green chemistry and considered to be eco-friendly (Yaqoob *et al*., 2020, Lomeli-Marroquin *et al*., 2019). In biological-mediated production of silver nanoparticles, the biomolecules cause the bio-reduction of silver cations in order to convert them into silver nanoparticles. The biomolecules also become attached to the silver nanoparticles surfaces thereby acting as stabilizing and capping agents (Barabadi *et al*. 2019).

Cancer is a collection of illnesses that metabolically and pathologically affect cells. It develops by a variety of processes, including metastasis, angiogenesis, and cell proliferation. Current cancer therapies have adverse side effects and affect normal cell functions in excessive exposure to drugs and radiation with silver nanoparticles evaluated for their use to improve the drug delivery and efficacy of chemotherapeutic drugs (Abdel-Fattah and Ali, 2018).

Green nanotechnology is eco-friendly, affordable and able to reduce metal ions and stabilize nanomaterials produced (Lomeli-Marroquin *et al*. 2019). Starch is made of amylopectin (70-80%) and amylose (20-30%) with the Hyacinth bean made up of mostly starch (48.66-51.02%). Porous starch is classified as modified starch granules having minute pores (± 1µm) varying in size and depth (Sujka *et al*. 2018, Zhang *et al*. 2012). There are various methods to synthesise porous starch using biological, physical and chemical means with solvent-exchange involving the dehydration of water on the starch granule surface using ethanol. Due to the greater surface area of starch granules, the more hydroxyl groups present result in more reactive sites to produce more pores (Han *et al*., 2020).

Functions of porous starches include improved adsorption and dissolution of poorly soluble drugs, as well as the ability to serve as carriers of various biological materials. The dissolution and bioavailability of paclitaxel (an anti-cancer drug) loaded into porous starch in the form of nanoparticles were compared to raw paclitaxel and paclitaxel loaded into porous starch in a study conducted by Wang *et al*. (2019). The nanoparticles loaded into the porous starch increased paclitaxel dissolution and bioavailability, implying a more effective mode of action for the anti-cancer medication. Therefore, in this study, porous starch prepared by solvent-exchange was used as a stabilizing and capping agent to synthesize silver nanoparticles, which were then characterized and tested for its potential as an eco-friendly, affordable method to synthesize a nutraceutical-based therapeutic delivery system against cancer.

4.2. Materials and methods

4.2.1. Native starch preparation

Lablab purpureus seeds were soaked overnight in NaOH, dehulled and dried. Seeds were then ground, sieved (180 µm) and the subsequent flour defatted and dried in a laminar flow. The powder was then diluted at 1:10 w/v in 0.025 mol/L Na_2SO_3. The composite was left at room temperature for approximately 1 hour before centrifugation (5 000 × *g* for 15 min), washing with ethanol and deionised water before freeze-drying (Mohan and Mellem, 2022)

4.2.2. Porous starch preparation

The method by Mohan and Mellem (2022) using a solvent-exchange technique was used for producing porous starch. In brief, 30 min were spent boiling 8% w/v of starch in distilled water while stirring. The starch slurry was placed into centrifuge tubes once it had cooled, kept at 5°C for an overnight storage period, and then frozen at -10°C. After being submerged in 95% ethanol for 24 h, the frozen starch had the ethanol evaporated using a rotary evaporator, thereafter it was freeze-dried.

4.2.3. Synthesis of silver nanoparticles (AgNPs)

With a few minor adjustments, the Lomeli-Marroquin *et al.* (2019) approach was used to create the silver nanoparticles. In brief, 1% w/v starch was agitated in boiling water for 30 min. Thereafter, the pH of the supernatant was adjusted to 11. After cooling, the solution was then centrifuged for 10 min at 10 000 × *g*. The starch solution was then mixed for 2 h at 70°C with 25 mM silver nitrate added in a 2:1 ratio. After the solution became dark brown, it was then centrifuged for 15 min at 10 000 × *g* and the pellet was utilised in the analysis.

4.2.4. Characterization of the silver nanoparticles

UV-visible spectroscopy

The nanoparticles were dissolved in distilled water (1:5 w/v), filtered through a Millipore filter (0.2 µM) then scanned in the range of 200-900 nm using a Cary60 spectrometer.

Zeta potential and size distribution

The particle size distribution and zeta potential were determined using a Litesizer 500 (Anton Paar) after samples were dissolved in distilled water (1:5 w/v) and filtered through a Millipore filter (0.2 µM).

Fourier-transform infrared spectroscopy (FTIR)

The chemical structure of nanoparticles were determined using an FTIR spectrophotometer (Cary 630, Agilent, CA, USA) with a spectrum range of 650-4 000 cm^{-1}. The spectrophotometer conducted 32 scans.

Transmission electron microscopy (TEM)

A Leica EM UC 7 microtome was used to section silver nanoparticles, and images from a Jeol 1010 TEM microscope were taken while the sections were cut.

4.2.5. Cytotoxicity

Cells were cultured at 37°C in a humidified incubator with 5% CO_2 using DMEM supplemented with 10% foetal calf serum and antibiotics (penicillin: 10000 U/mL, streptomycin sulphate: 10 000 U/mL). The medium of culture was changed every 2 d. Cells were trypsinized and subcultured after confluency. According to the method of Sipahli *et al*. (2020), cytotoxicity was assessed using the 3-(4,5 dimethylthiazol2-yl)-2,5-diphenyltetrazolium bromide (MTT) test. The cells were seeded ($1x10^2$ cells/mL) in a 96-well flat bottom plate and incubated for 24 h at 37°C (5% CO_2). After that, cells were exposed to 50 µL of a sample diluted to 5% DMSO (1 000-7.81 µg/mL) and incubated for 24 h. For the MTT assay, the positive control used was camptothecin, with untreated cells serving as the negative control. Cells were treated with a 20 µL aliquot of MTT solution (5 mg/mL) made in PBS, which was then incubated for 4 h at 37°C before 100 µL of DMSO was added. Using a microplate spectrophotometer (Multiscan Go, Thermo Scientific), the sample absorbance was then measured at 570 nm, and the % viability was calculated as follows:

$$\text{Cell viability } [\%] = \frac{\text{Absorbance of treated cells}}{\text{Absorbance of untreated cells}} \times 100 \quad \text{.....[1]}$$

4.2.6. Statistical analysis

Two-way analysis of variance (ANOVA) and Bonferroni's post hoc test were used to assess statistical differences in cell viability assays that were performed in triplicate. GraphPad Prism version 5.01 for Windows (GraphPad Software, San Diego, California, USA) was used to conduct the statistical analyses.

4.3. Results and discussion

Results obtained from this study have shown leguminous starch from Hyacinth bean to produce stable nanoparticles embedded in porous starch. Upon heating of the 1% porous starch solution to 70°C, 25 mM silver nitrate was added and the colour of the solution turned from clear to dark brown after 120 min under constant aggression.

The colour change obtained was in accordance with the excitation effect of surface plasmin resonance (Gomathi *et al.*, 2020, Satapathy *et al.*, 2013, Singh *et al.*, 2018). Starch has proven to have reducing properties, which are related to the presence of glucose units that form when starch is hydrolysed at high temperatures, and the ability of the glucose to oxidize into carboxylic acid, which results in the reduction of metallic ions to metal nanoparticles (Ortega-Arroyo *et al.*, 2013).

The hydroxyl groups present in starch, stabilize the silver nanoparticles through inter- and intramolecular hydrogen bonds which shows capping abilities (Lomeli-Marroquin *et al.* 2019). The UV-vis results revealed a peak at 425 nm (Figure 4.1) which correlates with the formation of silver nanoparticles (Abdulsahib 2021). However, these findings were higher than usually reported (420nm) but within the range (400-450 nm) of the typical surface plasmon resonance (SPR) of silver nanoparticles (Azizi *et al.*, 2017a, Azizi *et al.*, 2017b, Singh *et al.*, 2018). The peak at 425 nm was similar to those reported by Algotiml *et al.* (2022) which had peaks between 409-424 nm for the AgNPs. The peak is indicative of the reduction of silver ions to metallic silver nanoparticles and is formed due to the excitation of the free electrons in the AgNPs when absorbing visible light (Sarwer *et al.*, 2022, Suganthi *et al.*, 2019). The single peak shows that the AgNPs are spherical in shape and the broadness of the peak is indicative of the formation of poly dispersed AgNPs by using porous starch (Gomathi *et al.* 2020).

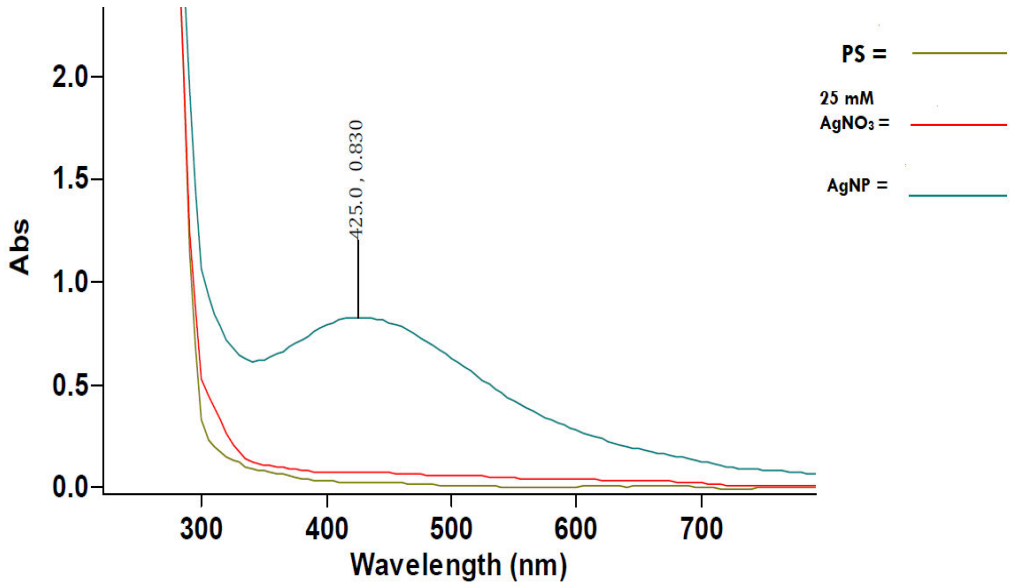

Figure 4.1: UV-vis spectra of silver nanoparticles (AgNP), porous starch (PS) and 25 mM silver nitrate ($AgNO_3$).

The TEM images (Figure 4.2) revealed the shape and size of the AgNPs, such as the spherical and sub-rounded shape as well as the dark spots (indicated with red arrows) inside which shows the porous starch encapsulating the silver nanoparticle. The AgNPs were found to be approximately 50 nm in size with similar images reported by Singh *et al.* (2018) who produced silver nanoparticles using extracts from plants as well as Algotiml *et al.* (2022) who produced silver nanoparticles from Red sea marine algae which reported spherical, grey and dark points in stabilized AgNPs.

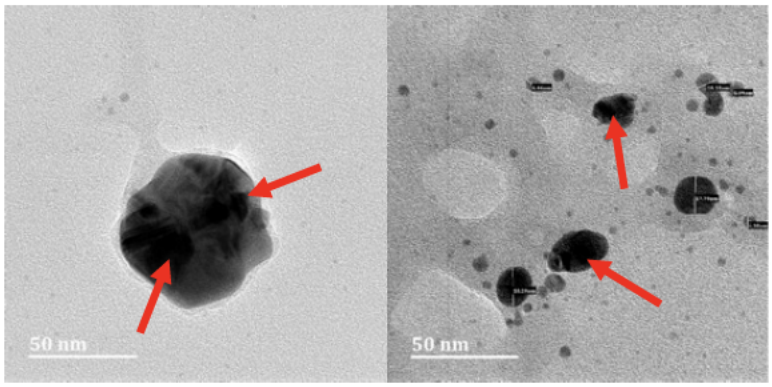

Figure 4.2: TEM images of silver nanoparticles.

The mean zeta-potential (Figure 4.3A) was -34.1±0.8 mV and the particle size distribution (Figure 4.3B) revealed two mean particle size diameter peaks at 187±69 and 16.2±2.6 nm. The zeta-potential determines the degree of electrostatic repulsion between particles that are similarly charged and next to each other in a solution (Azizi *et al.* 2017a). AgNPs are stable, twisted with anionic organic phases, and responsible for electrostatic stabilisation, according to the zeta-potential data (Azizi *et al.* 2017b). The zeta-potential was within the range that is typical of nanoparticles which is from +100 to -100 mV and is higher than the minimum of ±30 mV (Rajeshkumar and Bharath 2017).

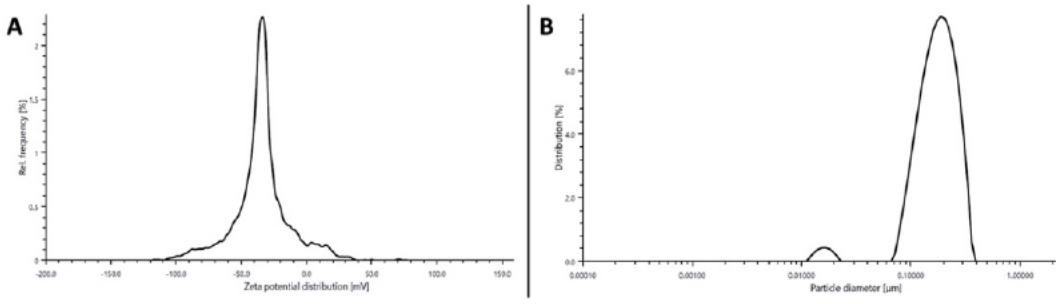

Figure 4.3: Zeta-potential distribution of silver nanoparticles [A] and particle size distribution of silver nanoparticles [B].

The FTIR spectra of the porous starch (PS), silver nanoparticles (AgNP) and 25 mM silver nitrate ($AgNO_3$) all show a broad band at 3280 cm^{-1} which is typical of the stretching of hydroxyl groups (Figure 4.4). The band around 2900 cm^{-1} in PS is due to the C-H bond stretching and the band at 1600 cm^{-1} in all spectra represents strong alkene bonds at C=C stretching (Algotiml *et al.*, 2022, Lomeli-Marroquin *et al.*, 2019, Singh *et al.*, 2018).

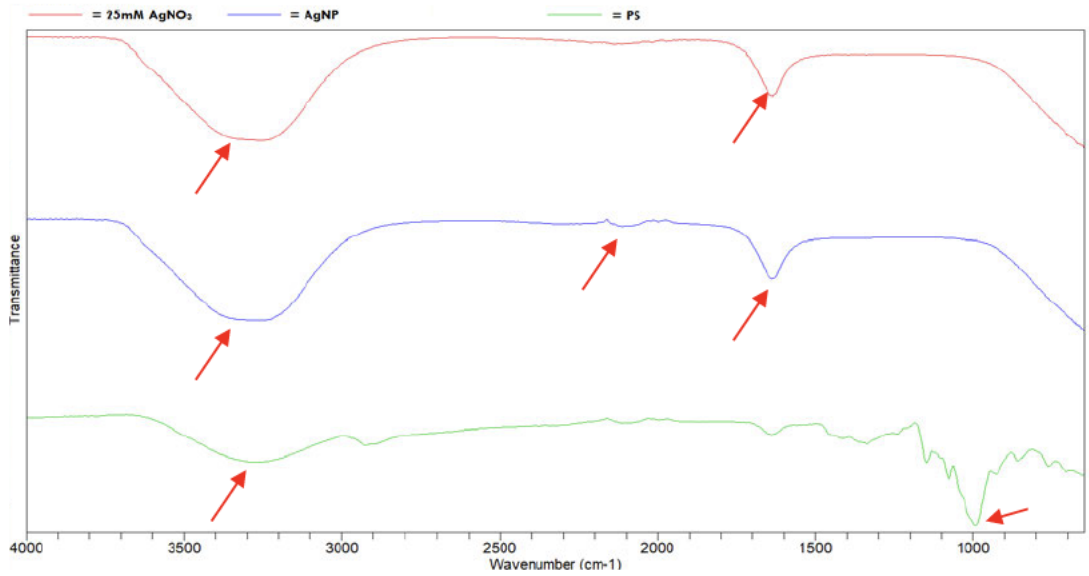

Figure 4.4: FTIR spectra of silver nanoparticles (AgNP), porous starch (PS) and 25 mM silver nitrate ($AgNO_3$).

The MTT assay was used to determine whether the porous starch (PS), 25 mM silver nitrate ($AgNO_3$), and the silver nanoparticles embedded in porous starch (AgNP) were able to limit the proliferation of cancerous cell lines CACO, MCF-7 and HELA (Figure 4.5). The cytotoxicity activity on cell growth was investigated at different concentrations (7.81-1000 µg/mL). The percentage viability was found to decrease for all compounds as the concentration increased, showing cytotoxicity to be dose-dependent (Liao *et al.*, 2019).

The IC50 values for the silver nanoparticles were 170.60; 38.31; 98.56 and 189.70 µg/mL for CACO, MCF-7, HELA and C2C12 cell lines, respectively. The silver nanoparticles showed minimal cytotoxic potential in all the cell lines. The low cytotoxicity activity of the silver nanoparticles may be dependent on various factors related to the variation of their size, concentration, shape, coatings, agglomeration, surface charges, etc. (Akter *et al.* 2018). Since the AgNPs had the highest overall cell viability in the muscular cell line (C2C12) this shows that the silver nanoparticles may have target specific behaviour and non-toxic nature in the presence of healthy cells (Azizi *et al.*, 2017b, Cai *et al.*, 2022).

The IC50 of the silver nanoparticles for the breast cancer cell line (MCF-7) was lower than the IC50 of camptothecin (45.76 µg/mL), thus showing greater cytotoxicity in the silver nanoparticles as compared to the chemo-preventative agent (Sipahli *et al.*, 2020).

The conditions in which the experiments were conducted may have contributed to the results shown. In a study investigating the doxorubicin-loaded carboxymethyl cellulose/starch/ ZnO nanocomposite hydrogel beads as an anticancer drug carrier agent, it was observed that the percentage cell viability decreased as the concentration increased which confirmed cytotoxicity (Gholamali and Yadollahi, 2020). Silver nanoparticles biosynthesized using a fruit shell had cytotoxicity against MCF-7 cell lines with the inhibitory concentration being 20 µg/mL (Gomathi *et al.*, 2020).

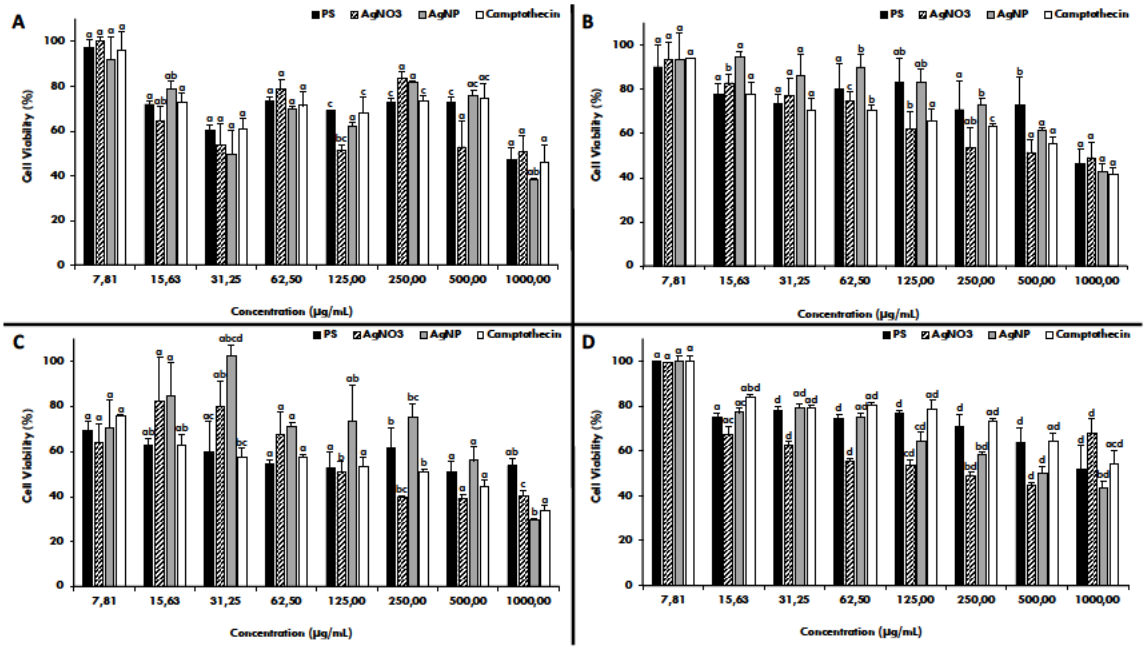

Figure 4.5: Cytotoxic potential of porous starch (PS), 25 mM silver nitrate ($AgNO_3$), silver nanoparticles (AgNP) and Camptothecin on HELA [A], CACO [B], C2C12 and MCF-7 [D] cells. Values with different letters are significantly different ($p < 0.05$) [n=3].

4.4. Conclusions

Based on the colour change, UV-Vis, and FTIR data, which also showed that the fabrication of the silver nanoparticles embedded in porous starch was effective, it was determined that the nanoparticles were stable. Porous starch may offer an effective, inexpensive, and environmentally acceptable way to create silver nanoparticles because chemical and physical processes are laborious, costly, and difficult. For CACO and HELA cancer cells, the silver nanoparticles displayed minimal cytotoxicity. This may be because of the concentration; possibly increasing the dosage might boost the cytotoxicity. Since the IC50 of the silver nanoparticles (38.31 g/mL) was lower than that of camptothecin (45.76 g/mL), the silver nanoparticles embedded in porous starch demonstrated cytotoxic potential in MCF-7 cells. Further research with *in vitro* apoptotic studies and key cancer enzymes are required to determine the anticancer activity and mechanism of action of the silver nanoparticles to improve their selectivity.

Chapter 5: General Discussion

Cancer is the second leading cause of death and a serious public health issue. Cancer detection and treatments were significantly delayed in 2020 as a result of the COVID-19 pandemic, which led to forecasts for 2023 of 1 958 310 additional cancer cases and 609 820 cancer deaths (Siegel *et al.*, 2023, Siegel *et al.*, 2019). The efficacy and the adverse effects of current treatments on patients had lead the increase in urgency for an effective, safe and affordable treatment for cancer (Abrahamse *et al.*, 2017, Adu *et al.*, 2023).

Due to their qualities, AgNPs are becoming more common and are employed in various sectors. To satisfy their needs, AgNPs have been created using a variety of techniques. Since biological methods have emerged as the most dependable, simple, effective, safe, and environmentally friendly method to synthesize silver nanoparticles with a definite morphology and size, the use of green chemistry to produce silver nanoparticles has enormous potential (Mahmud *et al.*, 2023). They also have antimicrobial, antibacterial, and anticancer abilities, however there is a risk of aggregation of silver ions from nanoparticles in the body, ultimately creating a poisonous environment. Therefore, to create stable silver nanoparticles, an adequate biopolymer is required as a capping agent (Arpan *et al.*, 2019, Restrepo and Villa, 2021).

The biopolymer starch has been mostly used as a reducing agent due to the C6 positions of the glucose unit providing hydroxyl groups to interact with silver ions and prevent aggregation (Restrepo and Villa, 2021). Starch has the highest content of carbohydrate in legume seeds (22-45%) (Ashogbon *et al.*, 2021). *Lablab purpureus* is a highly utilized crop that is unpopular providing a high source of starch (48.66-51.02%) and proteins (27.35-29.47%) and it is a drought-tolerant crop with some cultivars growing year-round (Maass *et al.*, 2010, Naiker *et al.*, 2020).

Although native starch has various useful properties, there are limitations to its abilities, therefore modifications to include pores to improve properties are needed (Mohan and Mellem, 2022). Porous biopolymers such as starch have improved properties such as high surface area and porosity, low density, biodegradability, biocompatibility, increased bioavailability amongst others (Ubeyitogullari *et al.*, 2022).

The first research chapter (Chapter 3) involved the investigation of different isolation techniques and their impact on the structural and physicochemical characteristics of porous starches from hyacinth bean and how they improved the properties of the native starch. The different methods were, firstly, solvent-exchange which involved the displacement of water from the starch gel with ethanol, creating a foam which thereby makes the starch porous. The second method was the freeze-thaw method, with the addition of mercaptosuccinic acid, a xerogel was produced. Lastly, the enzyme hydrolysis used α-amylase and amyloglucosidase to modify the starch granule integrity.

The characteristics of the native starch (NS), porous starches by solvent-exchange (SE); freeze-thaw (FT) and enzyme hydrolysis (EH) were observed using Fourier-transform infrared spectroscopy (FTIR), x-ray diffraction (XRD), differential scanning colorimetry (DSC), total starch determination and *in vitro* starch digestibility, amylose content, swelling power and solubility, pasting, and adsorption properties.

The structural characteristics of the SE and EH porous starches were similar to that of the native starch, with porous starch prepared by FT significantly different than NS in FTIR, XRD and pasting properties. This is most likely due to the presence of the mercaptosuccinic acid (Bao *et al.*, 2016). The FTIR spectra of the SE and EH showed the change in intensities revealing the presence of pores. The physicochemical characteristics of the porous starches had different trends. The total starches of SE and EH was higher than the NS. Resistant starch was present only in porous starch produced from SE with it being lower than NS. This may be due to the presence of pores on EH and FT causing the complete hydrolysis of the resistant starch. The starch digestibility is related to the amylose content and resistant starch, which controls the swelling capacity of the starch granules. The swelling capacity is dependent on the inter-molecular and intra-molecular bonds present in the starch chains (Bangar *et al.*, 2022).

The method utilized to create porous starch had a significant impact on both its physicochemical and structural characteristics. The porous starch samples made with SE and EH had many of the same structural and chemical properties as NS, however the addition of MSA to the freeze-thaw process significantly changed its properties. Given that FT has a greater solubility and a lower gelatinization property (DSC) than SE and EH, it would be advantageous for dye absorption.

Solvent-exchange and EH produced more positive findings, including improved adsorption, swelling, pasting, and gelatinization abilities, indicating that they have potential in being effective carriers in delivery systems and enhancing the adsorption of poorly soluble pharmaceuticals.

The physicochemical and structural characteristics, especially the presence of resistant starch, as well as the simplicity of the method to produce porous starch using solvent-exchange, strongly influenced the decision of using it as a reducing and capping agent in the synthesis of silver nanoparticles.

In the second research study, silver nanoparticles were produced using porous starch prepared by solvent-exchange and then characterised and tested for its cytotoxicity potential against colon cancer (CACO), breast cancer (MCF-7), cervical cancer (HELA) and muscle (C2C12) cell lines. The study aimed to determine the potential of silver nanoparticles embedded in porous starch (AgNP) as a therapeutic delivery system against cancer.

It was observed that the AgNP had a low inhibition concentration (IC_{50}) and high cell proliferation for the CACO and HELA cell lines. This may be due to the dosages, or problems during the growth of the cells. The AgNP had a lower IC_{50} for MCF-7 cancer cell line than that of Camptothecin. This showed promise as an anticancer treatment against breast cancer. Similarly, Khan *et al*. (2021) reported AgNPs, biosynthesized by using plant extract (*Heliotropium bacciferum*), having anticancer potential for MCF-7 and HCT-116 (colorectal) cancer cell lines. The study also revealed that the rise in production of ROS caused the cell death when treated with AgNPs. These results were also supported through a study by Valera-Zaragoza *et al*. (2020) who showed starch/AgNPs-3 composite to exhibit cytotoxic activity against MCF-7 cancer cells with minor deterioration to the healthy cells.

Chapter 6: Conclusion and recommendations

The research conducted represents the potential of porous starch from *Lablab purpureus* to synthesize, encapsulate and enhance the properties of silver nanoparticles for a therapeutic agent against cancer. Further research is required to understand and optimize the functionalities discovered in the silver nanoparticles embedded in porous starch study such as:

1. The porous starches have potential in use as carriers as well as biosynthesizing silver nanoparticles. Legume porous starches provide a reliable source of biopolymers that could be used to enhance adsorption abilities of compounds.
2. The silver nanoparticles cytotoxic abilities against breast cancer cells whilst leaving the normal cells unharmed and further apoptotic studies focussing on the *in vitro* and *in vivo* anti-cancer activity is recommended.

Chapter 7: References

ABDEL-FATTAH, W. I. & ALI, G. W. 2018. On the anti-cancer activities of silver nanoparticles. *Journal of Applied Biotechnology & Bioengineering,* 5, 43–46.

ABDULSAHIB, S. S. 2021. Synthesis, characterization and biomedical applications of silver nanoparticles. *Biomedicine,* 41, 458-464.

ABRAHAMSE, H., KRUGER, C. A., KADANYO, S. & MISHRA, A. 2017. Nanoparticles for Advanced Photodynamic Therapy of Cancer. *Photomedicine and Laser Surgery,* 35, 581-588.

ACEVEDO, B. A., VILLANUEVA, M., CHAVES, M. G., AVANZA, M. V. & RONDA, F. 2019. Starch enzymatic hydrolysis, structural, thermal and rheological properties of pigeon pea (*Cajanus cajan*) and dolichos bean (*Dolichos lab-lab*) legume starches. *International Journal of Food Science & Technology,* 55, 712-719.

ADU, O. T., NAIDOO, Y., LIN, J., DWARKA, D., MELLEM, J., MURTHY, H. N. & DEWIR, Y. H. 2023. Cytotoxic Potential of *Diospyros villosa* Leaves and Stem Bark Extracts and Their Silver Nanoparticles. *Plants (Basel),* 12, 769.

AGRAWAL, D. S. N. 2019. The Vital Phenomena of Apoptosis: A Review. *South Asian Research Journal of Medical Sciences,* 01, 15-19.

AHMED WANI, I., ALI WANI, A., GANI, A., MUZZAFFAR, S., KHALID GUL, M., AHMAD MASOODI, F. & AHMAD WANI, T. 2015. Effect of gamma-irradiation on physico-chemical and functional properties of arrowhead (*Sagittaria sagittifolia L.*) tuber flour. *Food Bioscience,* 11, 23-32.

AKPAPUNAM, M. 1996. Hyacinth bean (*Lablab purpureus* (L.) Sweet). *Legumes and Oilseeds in Nutrition*, 103-108.

AKTER, M., SIKDER, M. T., RAHMAN, M. M., ULLAH, A., HOSSAIN, K. F. B., BANIK, S., HOSOKAWA, T., SAITO, T. & KURASAKI, M. 2018. A systematic review on silver nanoparticles-induced cytotoxicity: Physicochemical properties and perspectives. *Journal of Advanced Research,* 9, 1-16.

AL-SNAFI & ESMAIL, A. 2017. The pharmacology and medical importance of Dolichos lablab (*Lablab purpureus*)- A review. *IOSR Journal of Pharmacy (IOSRPHR),* 07, 22-30.

ALGOTIML, R., GAB-ALLA, A., SEOUDI, R., ABULREESH, H. H., EL-READI, M. Z. & ELBANNA, K. 2022. Anticancer and antimicrobial activity of biosynthesized Red Sea marine algal silver nanoparticles. *Scientific Reports,* 12, 2421.

ALMATROUDI, A. 2020. Silver nanoparticles: synthesis, characterisation and biomedical applications. *Open Life Sciences,* 15, 819-839.

AMARAL, R. G., SEVERINO, P., SANTOS, S. A. D., ANDRADE, L. N. & CARVALHO, A. A. 2019. Natural Products as Treatment against Cancer: A Historical and Current Vision. *Clinics in Oncology,* 4, 1562.

ARPAN, D. B., ARINDAM, B. & ANSUMAN, C. 2019. Cytotoxic and mutagenic effects of green silver nanoparticles in cancer and normal cells: a brief review. *The Nucleus,* 62, 277-285.

ASHOGBON, A. O., AKINTAYO, E. T., OLADEBEYE, A. O., OLUWAFEMI, A. D., AKINSOLA, A. F. & IMANAH, O. E. 2021. Developments in the isolation, composition, and physicochemical properties of legume starches. *Critical Reviews in Food Science and Nutrition,* 61, 2938-2959.

AZIZI, M., GHOURCHIAN, H., YAZDIAN, F., BAGHERIFAM, S., BEKHRADNIA, S. & NYSTROM, B. 2017a. Anti-cancerous effect of albumin coated silver nanoparticles on MDA-MB 231 human breast cancer cell line. *Scientific Reports,* 7, 5178.

AZIZI, S., MOHAMAD, R., ABDUL RAHIM, R., MOHAMMADINEJAD, R. & BIN ARIFF, A. 2017b. Hydrogel beads bio-nanocomposite based on Kappa-Carrageenan and green synthesized silver nanoparticles for biomedical applications. *International Journal of Biological Macromolecules,* 104, 423-431.

BAJAJ, R., SINGH, N., KAUR, A. & INOUCHI, N. 2018. Structural, morphological, functional and digestibility properties of starches from cereals, tubers and legumes: a comparative study. *Journal of Food Science and Technology,* 55, 3799-3808.

BANGAR, S. P., ASHOGBON, A. O., LORENZO, J. M., PHIMOLSIRIPOL, Y. & CHAUDHARY, V. 2022. Recent advancements in properties, modifications, and applications of legume starches. *Journal of Food Processing and Preservation,* 46, e16997.

BAO, L., ZHU, X., DAI, H., TAO, Y., ZHOU, X., LIU, W. & KONG, Y. 2016. Synthesis of porous starch xerogels modified with mercaptosuccinic acid to remove hazardous gardenia yellow. *International Journal of Biological Macromolecules,* 89, 389-95.

BARABADI, H., VAHIDI, H., DAMAVANDI KAMALI, K., RASHEDI, M., HOSSEINI, O., GOLNARAGHI GHOMI, A. R. & SARAVANAN, M. 2019. Emerging Theranostic Silver Nanomaterials to Combat Colorectal Cancer: A Systematic Review. *Journal of Cluster Science,* 31, 311-321.

BENAVENT-GIL, Y. & ROSELL, C. M. 2017a. Morphological and physicochemical characterization of porous starches obtained from different botanical sources and amylolytic enzymes. *International Journal of Biological Macromolecules,* 103, 587-595.

BENAVENT-GIL, Y. & ROSELL, C. M. 2017b. Performance of Granular Starch with Controlled Pore Size during Hydrolysis with Digestive Enzymes. *Plant Foods and Human Nutrition* 72, 353-359.

BLACKADAR, C. B. 2016. Historical review of the causes of cancer. *World Journal of Clinic Oncology, 7*, 54-86.

BRAY, F., FERLAY, J., SOERJOMATARAM, I., SIEGEL, R. L., TORRE, L. A. & JEMAL, A. 2018. Global cancer statistics 2018: GLOBOCAN estimates of incidence and mortality worldwide for 36 cancers in 185 countries. *CA: A Cancer Journal for Clinicians,* 68, 394-424.

BUTTACAVOLI, M., ALBANESE, N. N., DI CARA, G., ALDUINA, R., FALERI, C., GALLO, M., PIZZOLANTI, G., GALLO, G., FEO, S., BALDI, F. & CANCEMI, P. 2018. Anticancer activity of biogenerated silver nanoparticles: an integrated proteomic investigation. *Oncotarget,* 9, 9685-9705.

CAI, Y., KARMAKAR, B., ALSALEM, H. S., EL-KOTT, A. F., BANI-FWAZ, M. Z., NEGM, S., OYOUNI, A. A. A., AL-AMER, O. & BATIHA, G. E.-S. 2022. Oak gum mediated green synthesis of silver nanoparticles under ultrasonic conditions: Characterization and evaluation of its antioxidant and anti-lung cancer effects. *Arabian Journal of Chemistry,* 15, 103848.

CANCER-RESEARCH-UK. 2023. *How cancers grow* [Online]. Available: https://www.cancerresearchuk.org/about-cancer/what-is-cancer/how-cancers-grow

CARNEIRO, B. A. & EL-DEIRY, W. S. 2020. Targeting apoptosis in cancer therapy. *Nature reviews, Clinical Oncology,* 17, 395-417.

CHAVEZ-MURILLO, C. E., VEYNA-TORRES, J. I., CAVAZOS-TAMEZ, L. M., DE LA ROSA-MILLAN, J. & SERNA-SALDIVAR, S. O. 2018. Physicochemical characteristics, ATR-FTIR molecular interactions and *in vitro* starch and protein digestion of thermally-treated whole pulse flours. *Food Research International,* 105, 371-383.

CHEN, G. & ZHANG, B. 2012. Hydrolysis of granular corn starch with controlled pore size. *Journal of Cereal Science,* 56, 316-320.

CHEN, J., WANG, Y., LIU, J. & XU, X. 2020. Preparation, characterization, physicochemical property and potential application of porous starch: A review. *International Journal of Biological Macromolecules,* 148, 1169-1181.

CHEN, L., MCCLEMENTS, D. J., ZHANG, H., ZHANG, Z., JIN, Z. & TIAN, Y. 2019. Impact of amylose content on structural changes and oil absorption of fried maize starches. *Food Chemistry,* 287, 28-37.

CHEN, X. Y., MA, X.W., WEN, J.Y., LIU, X.C., YU, X.R. & XIONG, F. 2021. Morphological, Structural and Functional Properties of Starches from Different Legume Resources. . *Legume Research-An International Journal,* 1, 6.

D'ARCY, M. S. 2019. Cell death: a review of the major forms of apoptosis, necrosis and autophagy. *Cell Biology International,* 43, 582-592.

DANG, T. L., THI & FRIBOURG-BLANC, ERIC & DANG, CHIEN 2012. Influence of surfactant on the preparation of silver nanoparticles by polyol method. *Advances in Natural Sciences: Nanoscience and Nanotechnology,* 3, 035004.

DENECKER, G., OVAERE, P., VANDENABEELE, P. & DECLERCQ, W. 2008. Caspase-14 reveals its secrets. *Journal of Cell Biology,* 180, 451-8.

DıBLAN, S., KADIROĞLU, P. & AYDEMIR, L. Y. 2018. Ft-Ir Spectroscopy Characterization and Chemometric Evaluation of Legumes Extracted with Different Solvents. *Food and Health*, 80-88.

DURA, A., BLASZCZAK, W. & ROSELL, C. M. 2014. Functionality of porous starch obtained by amylase or amyloglucosidase treatments. *Carbohydrate Polymers,* 101, 837-845.

DWARKA, D., THAVER;, V., NAIDU;, M., KOORBANALLY;, N. A. & BAIJNATH, A. H. 2017. *In vitro* chemo-preventative activity of *Strelitzia nicolai* aril extract containing bilirubin. *African Journal of Traditional, Complementary and Alternative Medicines,* 14, 147-156.

ELMORE, S. 2007. Apoptosis: a review of programmed cell death. *Toxicologic Pathology,* 35, 495-516.

FERLAY J, COLOMBET M, SOERJOMATARAM I, PARKIN DM, PIÑEROS M, ZNAOR A, BRAY F. 2021. Cancer statistics for the year 2020: An overview. Int J Cancer. Apr 5. doi: 10.1002/ijc.33588. Epub ahead of print. PMID: 33818764.

GAO, L., WU, Y., WAN, C., WANG, P., YANG, P., GAO, X., EECKHOUT, M. & GAO, J. 2022. Structural and physicochemical properties of pea starch affected by germination treatment. *Food Hydrocolloids,* 124, 107303.

GECER, E. N. 2023. Synthesis and characterization of silver nanoparticles using Origanum onites leaves: Cytotoxic, apoptotic, and necrotic effects on Capan-1, L929, and Caco-2 cell lines. *Green Processing and Synthesis,* 12, 20228126.

GHAVIMI, A. A., EBRAHIMZADEH, S., SHOKRGOZAR, M. H., SOLATI-HASHJIN, M. A., OSMAN, M. A. & AZUAN, N. 2015. Effect of starch content on the biodegradation of polycaprolactone/starch composite for fabricating in situ pore-forming scaffolds. *Polymer Testing,* 43, 94-102.

GHOLAMALI, I. & YADOLLAHI, M. 2020. Doxorubicin-loaded carboxymethyl cellulose/Starch/ZnO nanocomposite hydrogel beads as an anticancer drug carrier agent. *International Journal of Biological Macromolecules,* 160, 724-735.

GOMATHI, A. C., XAVIER RAJARATHINAM, S. R., MOHAMMED SADIQ, A. & RAJESHKUMAR, S. 2020. Anticancer activity of silver nanoparticles synthesized using aqueous fruit shell extract of Tamarindus indica on MCF-7 human breast cancer cell line. *Journal of Drug Delivery Science and Technology, 55*, 101376.

GUO, L., LI, G., LIU, J., MENG, Y. & TANG, Y. 2013. Adsorptive decolorization of methylene blue by crosslinked porous starch. *Carbohydrate Polymers,* 93, 374-9.

GUO, L., YUAN, Y., LI, J., TAN, C., JANASWAMY, S., LU, L., FANG, Y. & CUI, B. 2021. Comparison of functional properties of porous starches produced with different enzyme combinations. *International Journal of Biological Macromolecules,* 174, 110-119.

HABIB, H. M., THEURI, S. W., KHEADR, E. E. & MOHAMED, F. E. 2017. Functional, bioactive, biochemical, and physicochemical properties of the Dolichos lablab bean. *Food and Function,* 8, 872-880.

HAN, Z., HAN, Y., WANG, J., LIU, Z., BUCKOW, R. & CHENG, J. 2020. Effects of pulsed electric field treatment on the preparation and physicochemical properties of porous corn starch derived from enzymolysis. *Journal of Food Processing and Preservation,* 44, e14353.

HANAFI, M., QANNARI, E. & JAILLAIS, B. 2020. Multi-Block and Three-Way Data Analysis. In: Comprehensive Chemometrics *Elsevier*, 341-358.

HELLEDAY, T. 2017. Chemotherapy-induced toxicity-a secondary effect caused by released DNA? *Annals of Oncology,* 28, 2054-2055.

HEUZÉ, V., TRAN, G., SAUVANT, D., RENAUDEAU, D., BASTIANELLI, D. & LEBAS, F. 2016. *Lablab (Lablab purpureus)* [Online]. Available: http://www.feedipedia.org/node/297.

HOOVER, R., HUGHES, T., CHUNG, H. J. & LIU, Q. 2010. Composition, molecular structure, properties, and modification of pulse starches: A review. *Food Research International,* 43, 399-413.

HULL, R., FRANCIES, F. Z., OYOMNO, M. & DLAMINI, Z. 2020a. Colorectal Cancer Genetics, Incidence and Risk Factors: In Search for Targeted Therapies. *Cancer Management and Research,* 12, 9869-9882.

HULL, R., MBELE, M., MAKHAFOLA, T., HICKS, C., WANG, S. M., REIS, R. M., MEHROTRA, R., MKHIZE-KWITSHANA, Z., KIBIKI, G., BATES, D. O. & DLAMINI, Z. 2020b. Cervical cancer in low and middle-income countries. *Oncology Letters,* 20, 2058-2074.

HUY, T. Q., HUYEN, P. T. M., LE, A. T. & TONEZZER, M. 2020. Recent Advances of Silver Nanoparticles in Cancer Diagnosis and Treatment. *Anticancer Agents Med Chem,* 20, 1276-1287.

JARUCHALERMRAT, P. & NIAMLANG, S. 2021. Development of cornstarch-based hydrogel drug delivery patch controlled by the electric field for hypertension. *Journal of Physics: Conference Series,* 1719, 012074.

JOHNSON, S. B., PARK, H. S., GROSS, C. P. & YU, J. B. 2018. Complementary Medicine, Refusal of Conventional Cancer Therapy, and Survival Among Patients With Curable Cancers. *JAMA Oncology,* 4, 1375-1381.

JU, J., CHEN, X., XIE, Y., YU, H., CHENG, Y., QIAN, H. & YAO, W. 2019. Simple microencapsulation of plant essential oil in porous starch granules: Adsorption kinetics and antibacterial activity evaluation. *Journal of Food Processing and Preservation,* 43, e14156.

JURJ, A., BRAICU, C., POP, L. A., TOMULEASA, C., GHERMAN, C. D. & BERINDAN-NEAGOE, I. 2017. The new era of nanotechnology, an alternative to change cancer treatment. *Drug Design, Development and Therapy,* 11, 2871-2890.

KAUFMAN, R. C., WILSON, J. D., BEAN, S. R., HERALD, T. J. & SHI, Y. C. 2015. Development of a 96-well plate iodine binding assay for amylose content determination. *Carbohydrate Polymers,* 115, 444-447.

KHAN, M. S., ALOMARI, A., TABREZ, S., HASSAN, I., WAHAB, R., BHAT, S. A., ALAFALEQ, N. O., ALTWAIJRY, N., SHAIK, G. M., ZAIDI, S. K., NOUH, W., ALOKAIL, M. S. & ISMAEL, M. A. 2021. Anticancer Potential of Biogenic Silver Nanoparticles: A Mechanistic Study. *Pharmaceutics,* 13, 707.

KHORRAMI, S., ZAREPOUR, A. & ZARRABI, A. 2019. Green synthesis of silver nanoparticles at low temperature in a fast pace with unique DPPH radical scavenging and selective cytotoxicity against MCF-7 and BT-20 tumor cell lines. *Biotechnology Reports,* 24, e00393.

KILONZI, S. M., MAKOKHA, A. O. & KENJI, G. M. 2017. Physical characteristics, proximate composition and anti-nutritional factors in grains of lablab bean (*Lablab purpureus*) genotypes from Kenya. *Journal of Applied Biosciences,* 114, 11289.

KOKILA, S., D'SOUZA, M. R. & DEVARAJ, V. R. 2014. Response of *Lablab purpureus* (Hyacinth bean) cultivars to drought stress. *Asian Journal of Plant Science and Research,* 4, 48-55.

LACERDA, L. D., LEITE, D. C., SOARES, R. M. D. & DA SILVEIRA, N. P. 2018. Effects of α-Amylase, Amyloglucosidase, and Their Mixture on Hierarchical Porosity of Rice Starch. *Starch - Stärke,* 70, 1800008.

LEHMANN, U. & ROBIN, F. 2007. Slowly digestible starch – its structure and health implications: a review. *Trends in Food Science & Technology,* 18, 346-355.

LI, Y., GUO, M., LIN, Z., ZHAO, M., XIAO, M., WANG, C., XU, T., CHEN, T. & ZHU, B. 2016. Polyethylenimine-functionalized silver nanoparticle-based co-delivery of paclitaxel to induce HepG2 cell apoptosis. *International Journal of Nanomedicine,* 11, 6693-6702.

LIAO, C., LI, Y. & TJONG, S. C. 2019. Bactericidal and Cytotoxic Properties of Silver Nanoparticles. *International Journal of Molecular Sciences,* 20, 449.

LIN, S. R., FU, Y. S., TSAI, M. J., CHENG, H. & WENG, C. F. 2017. Natural Compounds from Herbs that can Potentially Execute as Autophagy Inducers for Cancer Therapy. *International Journal of Molecular Sciences,* 18, 1412.

LIOU, G. Y. & STORZ, P. 2010. Reactive oxygen species in cancer. *Free Radical Research,* 44, 479-96.

LIU J. and POPE C. N. 2020. Intrinsic and extrinsic factors that can modify toxicity. *An Introduction to Interdisciplinary Toxicology*, 285-293.

LIU, L., SHEN, W., ZHANG, W., LI, F. & ZHU, Z. 2018. Porous Starch and Its Applications. *Functional Starch and Applications in Food*, 91-117.

LIU, X., SHAN, K., SHAO, X., SHI, X., HE, Y., LIU, Z., JACOB, J. A. & DENG, L. 2021. Nanotoxic Effects of Silver Nanoparticles on Normal HEK-293 Cells in Comparison to Cancerous HeLa Cell Line. *International Journal of Nanomedicine,* 16, 753-761.

LOMELI-MARROQUIN, D., MEDINA CRUZ, D., NIETO-ARGUELLO, A., VERNET CRUA, A., CHEN, J., TORRES-CASTRO, A., WEBSTER, T. J. & CHOLULA-DIAZ, J. L. 2019. Starch-mediated synthesis of mono- and bimetallic silver/gold nanoparticles as antimicrobial and anticancer agents. *International Journal of Nanomedicine,* 14, 2171-2190.

MAASS, B. L., KNOX, M. R., VENKATESHA, S. C., ANGESSA, T. T., RAMME, S. & PENGELLY, B. C. 2010. Lablab purpureus-A Crop Lost for Africa? *Tropical Plant Biology,* 3, 123-135.

MADE, F., WILSON, K., JINA, R., TLOTLENG, N., JACK, S., NTLEBI, V. & KOOTBODIEN, T. 2017. Distribution of cancer mortality rates by province in South Africa. *Cancer Epidemiology,* 51, 56-61.

MAHMUD, F. B., M, M., UJ, K., KRISHNASAMY, D., CHEBWOGEN, S., RAMESH, V., WIJEKOOM, D. G. W. M. H. M. M. & SENEVIRATHNE, H. 2023. A Review On Silver Nanoparticles And Its Role In Treating Diseases: Anticancer Activity Of Agnps. *International Research Journal of Modernization in Engineering Technology and Science*, 2582-5208.

MAJZOOBI, M., HEDAYATI, S. & FARAHNAKY, A. 2015. Functional properties of microporous wheat starch produced by α-amylase and sonication. *Food Bioscience,* 11, 79-84.

MALTSER, S., CRISTIAN, A., SILVER, J. K., MORRIS, G. S. & STOUT, N. L. 2017. A Focused Review of Safety Considerations in Cancer Rehabilitation. *PM R,* 9, S415-S428.

MANICKAVASAGAN, A. & THIRUNATHAN, P. eds 2020. *Pulses: processing and product development*. Springer Nature.

MAO, J. J., PILLAI, G. G., ANDRADE, C. J., LIGIBEL, J. A., BASU, P., COHEN, L., KHAN, I. A., MUSTIAN, K. M., PUTHIYEDATH, R., DHIMAN, K. S., LAO, L., GHELMAN, R., CACERES

GUIDO, P., LOPEZ, G., GALLEGO-PEREZ, D. F. & SALICRUP, L. A. 2022. Integrative oncology: Addressing the global challenges of cancer prevention and treatment. *CA: A Cancer Journal for Clinicians,* 72, 144-164.

MOHAN, N. & MELLEM, J. J. 2020. Functional properties of the protein isolates of hyacinth bean [Lablab purpureus (L.) Sweet]: An effect of the used procedures. *LWT - Food Science and Technology,* 129, 109572.

MOHAN, N. & MELLEM, J. J. 2022. Structural and physicochemical characterization of porous starch prepared by enzymatic hydrolysis, solvent-exchange, and freeze–thaw cross-linking treatments. *International Journal of Food Science & Technology,* 57, 2356-2364.

NAEEM, M., SHABBIR, A., ANSARI, A. A., AFTAB, T., KHAN, M. M. A. & UDDIN, M. 2020. Hyacinth bean (*Lablab purpureus* L.) – An underutilised crop with future potential. *Scientia Horticulturae,* 272, 109551.

NAIKER, T. S., BAIJNATH, H., AMONSOU, E. O. & MELLEM, J. J. 2020. The effect of soaking, steaming, and dehydration on the microstructure, physicochemical properties and in vitro starch digestibility of flour produced from *Lablab purpureus* (L.) Sweet (hyacinth bean). *Journal of Food Processing and Preservation*, e14430.

NAIKER, T. S., GERRANO, A. & MELLEM, J. 2019. Physicochemical properties of flour produced from different cowpea (*Vigna unguiculata*) cultivars of Southern African origin. *Journal of Food Science and Technology,* 56, 1541-1550.

NING, P., LU, S., BAI, X., WU, X., GAO, C., WEN, N. & LIU, M. 2018. High encapsulation and localized delivery of curcumin from an injectable hydrogel. *Materials Science & Engineering C,* 83, 121-129.

NUSSBAUMER, S., BONNABRY, P., VEUTHEY, J. L. & FLEURY-SOUVERAIN, S. 2011. Analysis of anticancer drugs: a review. *Talanta,* 85, 2265-89.

NWAGU, G. C., BHATTARAI, S., SWAHN, M., AHMED, S. & ANEJA, R. 2021. Prevalence and Mortality of Triple-Negative Breast Cancer in West Africa: Biologic and Sociocultural Factors. *JCO Global Oncology* 7, 1129-1140.

NWOKOCHA, L. M., SOETAN, K. O. & WILLIAMS, P. A. 2010. A study of the properties of starch isolated from three varieties of Lablab purpureus seeds. *Carbohydrate Polymers,* 79, 685-693.

OBENG, E. 2021. Apoptosis (programmed cell death) and its signals - A review. *Brazilian Journal of Biology,* 81, 1133-1143.

OLIYAEI, N., MOOSAVI-NASAB, M., TAMADDON, A. M. & FAZAELI, M. 2020. Encapsulation of fucoxanthin in binary matrices of porous starch and halloysite. *Food Hydrocolloids,* 100, 105458.

ORTEGA-ARROYO, L., MARTIN-MARTINEZ, E. S., AGUILAR-MENDEZ, M. A., CRUZ-OREA, A., HERNANDEZ-PE´REZ, I. & GLORIEUX, C. 2013. Green synthesis method of silver nanoparticles using starch as capping agent applied. *Starch/Sta¨rke,* 65, 814–821.

PATIL, R. S., KOKATE, M. R., JAMBHALE, C. L., PAWAR, S. M., HAN, S. H. & KOLEKAR, S. S. 2012. One-pot synthesis of PVA-capped silver nanoparticles their characterization and biomedical application. *Advances in Natural Sciences: Nanoscience and Nanotechnology,* 3, 015013.

PHILLIPS, R. D. 1993. Starchy legumes in human nutrition, health and culture. *Plant Foods for Human Nutrition,* 44, 195-211.

PUNYANITYA, S., KOONAWOOT, R., RUKSANTI, A., THIENSEM, S., RAKSUJARIT, A. & SONTICHAI, W. 2017. *In Vivo* Clinical Trial of Porous Starch-Hydroxyapatite Composite Biomaterials for Bone Regeneration. *Key Engineering Materials,* 744, 480-484.

QI, X. & TESTER, R. F. 2019. Starch granules as active guest molecules or microorganism delivery systems. *Food Chemistry,* 271, 182-186.

QIAN, C. & MCCLEMENTS, D. J. 2011. Formation of nanoemulsions stabilized by model food-grade emulsifiers using high-pressure homogenization: Factors affecting particle size. *Food Hydrocolloids,* 25, 1000-1008.

RAJESHKUMAR, S. & BHARATH, L. V. 2017. Mechanism of plant-mediated synthesis of silver nanoparticles - A review on biomolecules involved, characterisation and antibacterial activity. *Chemico-Biological Interactions,* 273, 219-227.

RAMKISSON, S., DWARKA, D., VENTER, S. & MELLEM, J. J. 2020. *In vitro* anticancer and antioxidant potential of *Amaranthus cruentus* protein and its hydrolysates. *Food Science and Technology,* 40, 634-639.

RAMSOOKMOHAN, S., VENTER, S. & MELLEM, J. J. 2020. The effect of processing on the physicochemical properties and amino acid profile of flour from *Amaranthus cruentus*. *Journal of Food Processing and Preservation*, 14677.

RATHER, R. A. & BHAGAT, M. 2018. Cancer Chemoprevention and Piperine: Molecular Mechanisms and Therapeutic Opportunities. *Frontiers in Cell and Developmental Biology,* 6, 10.

RENGADU, D., GERRANO, A. S. & MELLEM, J. J. 2020. Physicochemical and structural characterization of resistant starch isolated from *Vigna unguiculata*. *International Journal of Biological Macromolecules,* 147, 268-275.

RESTREPO, C. V. & VILLA, C. C. 2021. Synthesis of silver nanoparticles, influence of capping agents, and dependence on size and shape: A review. *Environmental Nanotechnology, Monitoring & Management*, 100428.

RISS, T., NILES, A., MORAVEC, R., KARASSINA, N. & VIDUGIRIENE, J. 2019. *Cytotoxicity Assays: In Vitro Methods to Measure Dead Cells* [Online]. Bethesda (MD): Eli Lilly & Company and the National Center for Advancing Translational Sciences. Available: https://www.ncbi.nlm.nih.gov/books/.

ROSTAMABADI, H., FALSAFI, S. R. & JAFARI, S. M. 2019. Starch-based nanocarriers as cutting-edge natural cargos for nutraceutical delivery. *Trends in Food Science & Technology,* 88, 397-415.

SARAVANAKUMAR, K., SRIRAM, B., SATHIYASEELAN, A., MARIADOSS, A. V. A., HU, X., HAN, K. S., VISHNUPRIYA, V., MUBARAKALI, D. & WANG, M. H. 2021. Synthesis, characterization, and cytotoxicity of starch-encapsulated biogenic silver nanoparticle and its improved anti-bacterial activity. *International Journal of Biological Macromolecules,* 182, 1409-1418.

SARWER, Q., AMJAD, M. S., MEHMOOD, A., BINISH, Z., MUSTAFA, G., FAROOQ, A., QASEEM, M. F., ABASI, F. & PEREZ DE LA LASTRA, J. M. 2022. Green Synthesis and Characterization of Silver Nanoparticles Using *Myrsine africana* Leaf Extract for Their Antibacterial, Antioxidant and Phytotoxic Activities. *Molecules,* 27, 7612.

SATAPATHY, S. R., MOHAPATRA, P., PREET, R., DAS, D., SARKAR, B., CHOUDHURI, T., WYATT, M. D. & KUNDU, C. N. 2013. Silver-based nanoparticles induce apoptosis in human colon cancer cells mediated through p53. *Nanomedicine (Lond),* 8, 1307-22.

SIEGEL, R. L., MILLER, K. D. & JEMAL, A. 2019. Cancer statistics, 2019. *CA: A Cancer Journal for Clinicians,* 69, 7-34.

SIEGEL, R. L., MILLER, K. D., WAGLE, N. S. & JEMAL, A. 2023. Cancer statistics, 2023. *CA: A Cancer Journal for Clinicians,* 73, 17-48.

SINGH, J., DARTOIS, A. & KAUR, L. 2010. Starch digestibility in food matrix: a review. *Trends in Food Science & Technology,* 21, 168-180.

SINGH, K., NAIDOO, Y., MOCKTAR, C. & BAIJNATH, H. 2018. Biosynthesis of silver nanoparticles using Plumbago auriculata leaf and calyx extracts and evaluation of their antimicrobial activities. *Advances in Natural Sciences: Nanoscience and Nanotechnology,* 9, 035004.

SIPAHLI, S., DWARKA, D., AMONSOU, E. & MELLEM, J. 2020. I*n vitro* antioxidant and apoptotic activity of *Lablab purpureus* (L.) Sweet isolate and hydrolysates. *Food Science and Technology,* 42, e55220.

SIVAMARUTHI, B. S., NALLASAMY, P. K., SUGANTHY, N., KESIKA, P. & CHAIYASUT, C. 2022. Pharmaceutical and biomedical applications of starch-based drug delivery system: A review. *Journal of Drug Delivery Science and Technology,* 77, 103890.

SUGANTHI, S., VIGNESH, S., MOHANAPRIYA, S., SUNDAR, J. K. & RAJ, V. 2019. Microwave-assisted synthesis of l-histidine capped silver nanoparticles for enhanced photocatalytic activity under visible light and effectual antibacterial performance. *Journal of Materials Science: Materials in Electronics,* 30, 15168–15183.

SUNG H, FERLAY J, SIEGEL RL, LAVERSANNE M, SOERJOMATARAM I, JEMAL A, BRAY F. 2021. Global cancer statistics 2020: GLOBOCAN estimates of incidence and mortality worldwide for 36 cancers in 185 countries. *CA Cancer Journal for Clinicians.* 71: 209-249.

SUJKA, M., PANKIEWICZ, U., KOWALSKI, R., NOWOSAD, K. & NOSZCZYK-NOWAK, A. 2018. Porous starch and its application in drug delivery systems. *Polymers in Medicine,* 48, 25-29.

TAYADE, R., KULKARNI, K. P., JO, H., SONG, J. T. & LEE, J. D. 2019. Insight Into the Prospects for the Improvement of Seed Starch in Legume-A Review. *Frontiers in Plant Science,* 10, 1213.

THUMBRAIN, D., DWARKA, D., GERRANO, A. S. & MELLEM, J. J. 2020. Antioxidant and apoptotic potential of protein isolates derived from *Vigna unguiculata* (L.) Walp. *International Journal of Food Science & Technology, 55*, 2813-2823.

TSUJI, T., KAKITA, T. & TSUJI, M. 2002. Preparation of nano-size particles of silver with femtosecond laser ablation in water. *Applied Surface Science*, 314-320.

UBEYITOGULLARI, A., AHMADZADEH, S., KANDHOLA, G. & KIM, J. W. 2022. Polysaccharide-based porous biopolymers for enhanced bioaccessibility and bioavailability of bioactive food compounds: Challenges, advances, and opportunities. *Comprehensive reviews in food science and food safety,* 21, 4610-4639.

VALERA-ZARAGOZA, M., HUERTA-HEREDIA, A. A., PEÑA-RICO, M. A., JUAREZ-ARELLANO, E. A., NAVARRO-MTZ, A. K., RAMÍREZ-VARGAS, E. & SÁNCHEZ-VALDES, S. 2020. Morphological, structural and cytotoxic behavior of starch/silver nanocomposites with synthesized silver nanoparticles using *Stevia rebaudiana* extracts. *Polymer Bulletin,* 78, 1683-1701.

VERMA, A. K., JYOTHI, K. U. & RAO, A. V. D. D. 2014. Genetic variability, heritability and genetic advance studies in Dolichos bean (*Lablab purpureus* L.) genotypes. *Electronic Journal of Plant Breeding*, 272-276.

VERMA, R., JAN, S., RANI, S., JAN, K., SWER, T. L., PRAKASH, K. S., DAR, M. Z. & BASHIR, K. 2018. Physicochemical and functional properties of gamma irradiated buckwheat and potato starch. *Radiation Physics and Chemistry,* 144, 37-42.

VLĂSCEANU, G. M., MARIN, Ș., ȚIPLEA, R. E., BUCUR, I. R., LEMNARU, M., MARIN, M. M., GRUMEZESCU, A. M. & ANDRONESCU, E. 2016. Silver nanoparticles in cancer therapy. *Nanobiomaterials in Cancer Therapy*, 29-56.

WANG, L., ZHAO, X., YANG, F., WU, W., WU, M., LI, Y. & ZHANG, X. 2019. Loading paclitaxel into porous starch in the form of nanoparticles to improve its dissolution and bioavailability. *International Journal of Biological Macromolecules,* 138, 207-214.

WANG, X., YUAN, L., DENG, H. & ZHANG, Z. 2021. Structural characterization and stability study of green synthesized starch stabilized silver nanoparticles loaded with isoorientin. *Food Chemistry,* 338, 127807.

WANI, I. A., SOGI, D. S., HAMDANI, A. M., GANI, A., BHAT, N. A. & SHAH, A. 2016. Isolation, composition, and physicochemical properties of starch from legumes: A review. *Starch - Stärke,* 68, 834-845.

WHISTLER, R. L., BEMILLER, J. N. & PASCHALL, E. F. 2012. *Starch: Chemistry and Technology*, Elsevier Science.

WHO, W. H. O. 2020. WHO report on cancer: setting priorities, investing wisely and providing care for all.

WORLD-HEALTH-ORGANIZATION. 2023. *Colorectal cancer* [Online]. Available: https://www.who.int/news-room/fact-sheets/detail/colorectal-cancer.

WU, C., WANG, Z., ZHI, Z., JIANG, T., ZHANG, J. & WANG, S. 2011. Development of biodegradable porous starch foam for improving oral delivery of poorly water soluble drugs. International Journal of Pharmaceutics, 403, 162-9.

WU, W., JIAO, A., XU, E., CHEN, Y., JIN, Z. 2020. Effects of Extrusion Technology Combined with Enzymatic Hydrolysis on the Structural and Physicochemical Properties of Porous Corn Starch. Food and Bioprocess Technology, 13, 442–451.

WYPIJ, M., JEDRZEJEWSKI, T., TRZCINSKA-WENCEL, J., OSTROWSKI, M., RAI, M. & GOLINSKA, P. 2021. Green Synthesized Silver Nanoparticles: Antibacterial and Anticancer Activities, Biocompatibility, and Analyses of Surface-Attached Proteins. *Frontiers in Microbiology,* 12, 632505.

XI, C., ZHU, L., ZHUANG, Y., WANG, S., SUN, G., LIU, Y. & WANG, D. 2018. Experimental Evaluation of Tranexamic Acid-Loaded Porous Starch as a Hemostatic Powder. *Clinical and Applied Thrombosis/Hemostasis,* 24, 279-286.

YAQOOB, A. A., UMAR, K. & IBRAHIM, M. N. M. 2020. Silver nanoparticles: various methods of synthesis, size affecting factors and their potential applications–a review. *Applied Nanoscience,* 10, 1369-1378.

ZHANG, B., CUI, D., LIU, M., GONG, H., HUANG, Y. & HAN, F. 2012. Corn porous starch: preparation, characterization and adsorption property. *International Journal of Biological Macromolecules,* 50, 250-6.

ZHANG, Q., LIU, J., ZHANG, M., WEI, S., LI, R., GAO, Y., PENG, W. & WU, C. 2019. Apoptosis Induction of Fibroblast-Like Synoviocytes Is an Important Molecular-Mechanism for Herbal Medicine along with its Active Components in Treating Rheumatoid Arthritis. *Biomolecules,* 9, 795.

ZHANG, X. F., LIU, Z. G., SHEN, W. & GURUNATHAN, S. 2016. Silver Nanoparticles: Synthesis, Characterization, Properties, Applications, and Therapeutic Approaches. *International Journal of Molecular Sciences,* 17, 1534.

ZHANG, Z., HUANG, J., JIANG, S., LIU, Z., GU, W., YU, H. & LI, Y. 2013. Porous starch based self-assembled nano-delivery system improves the oral absorption of lipophilic drug. *International Journal of Pharmaceutics,* 444, 162-168.

ZHAO, A.-Q., YU, L., YANG, M., WANG, C.-J., WANG, M.-M. & BAI, X. 2018. Effects of the combination of freeze-thawing and enzymatic hydrolysis on the microstructure and physicochemical properties of porous corn starch. *Food Hydrocolloids,* 83, 465-472.

ZHU, J., ZHONG, L., CHEN, W., SONG, Y., QIAN, Z., CAO, X., HUANG, Q., ZHANG, B., CHEN, H. & CHEN, W. 2019. Preparation and characterization of pectin/chitosan beads containing porous starch embedded with doxorubicin hydrochloride: A novel and simple colon targeted drug delivery system. *Food Hydrocolloids,* 95, 562-570.